
Walsh-Hadamard Variational Inference for Bayesian Deep Learning

Simone Rossi*

Data Science Department
EURECOM (FR)
simone.rossi@eurecom.fr

Sébastien Marmin*

Data Science Department
EURECOM (FR)
sebastien.marmin@eurecom.fr

Maurizio Filippone

Data Science Department
EURECOM (FR)
maurizio.filippone@eurecom.fr

Abstract

Over-parameterized models, such as DeepNets and ConvNets, form a class of models that are routinely adopted in a wide variety of applications, and for which Bayesian inference is desirable but extremely challenging. Variational inference offers the tools to tackle this challenge in a scalable way and with some degree of flexibility on the approximation, but for over-parameterized models this is challenging due to the over-regularization property of the variational objective. Inspired by the literature on kernel methods, and in particular on structured approximations of distributions of random matrices, this paper proposes Walsh-Hadamard Variational Inference (WHVI), which uses Walsh-Hadamard-based factorization strategies to reduce the parameterization and accelerate computations, thus avoiding over-regularization issues with the variational objective. Extensive theoretical and empirical analyses demonstrate that WHVI yields considerable speedups and model reductions compared to other techniques to carry out approximate inference for over-parameterized models, and ultimately show how advances in kernel methods can be translated into advances in approximate Bayesian inference for Deep Learning.

1 Introduction

Since its inception, Variational Inference (VI, [26]) has continuously gained popularity as a scalable and flexible approximate inference scheme for a variety of models for which exact Bayesian inference is intractable. Bayesian neural networks [37, 41] represent a good example of models for which inference is intractable, and for which VI– and approximate inference in general – is challenging due to the nontrivial form of the posterior distribution and the large dimensionality of the parameter space [18, 15]. Recent advances in VI allow one to effectively deal with these issues in various ways. For instance, a flexible class of posterior approximations can be constructed using, e.g., normalizing flows [49], whereas the need to operate with large parameter spaces has pushed the research in the direction of Bayesian compression [36, 39].

Employing VI is notoriously challenging for over-parameterized statistical models. In this paper, we focus in particular on Bayesian Deep Neural Networks (DNNS) and Bayesian Convolutional Neural Networks (CNNs) as typical examples of over-parameterized models. Let’s consider a supervised

learning task with N input vectors and corresponding labels collected in $\mathbf{X} = \{\mathbf{x}_1, \dots, \mathbf{x}_N\}$ and $\mathbf{Y} = \{\mathbf{y}_1, \dots, \mathbf{y}_N\}$, respectively; furthermore, let's consider DNNs with weight matrices $\mathbf{W} = \{\mathbf{W}^{(1)}, \dots, \mathbf{W}^{(L)}\}$, likelihood $p(\mathbf{Y}|\mathbf{X}, \mathbf{W})$, and prior $p(\mathbf{W})$. Following standard variational arguments, after introducing an approximation $q(\mathbf{W})$ to the posterior $p(\mathbf{W}|\mathbf{X}, \mathbf{Y})$ it is possible to obtain a lower bound to the log-marginal likelihood $\log [p(\mathbf{Y}|\mathbf{X})]$ as follows:

$$\log [p(\mathbf{Y}|\mathbf{X})] \geq \mathbb{E}_{q(\mathbf{W})}[\log p(\mathbf{Y}|\mathbf{X}, \mathbf{W})] - \text{KL}\{q(\mathbf{W})\|p(\mathbf{W})\}. \quad (1)$$

The first term acts as a model fitting term, whereas the second one acts as a regularizer, penalizing solutions where the posterior is far away from the prior. It is easy to verify that the KL term can be the dominant one in the objective for over-parameterized models. For example, a mean field posterior approximation turns the KL term into a sum of as many KL terms as the number of model parameters, say Q , which can dominate the overall objective when $Q \gg N$. As a result, the optimization focuses on keeping the approximate posterior close to the prior, disregarding the rather important model fitting term. This issue has been observed in a variety of deep models [3], where it was proposed to gradually include the KL term throughout the optimization [3, 53] to scale up the model fitting term [62, 61] or to improve the initialization of variational parameters [50]. Alternatively, other approximate inference methods for deep models with connections to VI have been proposed, notably Monte Carlo Dropout [MCD; 15] and Noisy Natural Gradients [NNG; 66].

In this paper, we propose a novel strategy to cope with model over-parameterization when using variational inference, which is inspired by the literature on kernel methods. Our proposal is to reparameterize the variational posterior over model parameters by means of a structured decomposition based on random matrix theory [58], which has inspired a number of fundamental contributions in the literature on approximations for kernel methods, such as FASTFOOD [33] and Orthogonal Random Features (ORF, [64]). The key operation within our proposal is the Walsh-Hadamard transform, and this is why we name our proposal Walsh-Hadamard Variational Inference (WHVI).

Without loss of generality, consider Bayesian DNNs with weight matrices $\mathbf{W}^{(l)}$ of size $D \times D$. Compared with mean field VI, WHVI has a number of attractive properties. The number of parameters is reduced from $\mathcal{O}(D^2)$ to $\mathcal{O}(D)$, thus reducing the over-regularization effect of the KL term in the variational objective. We derive expressions for the reparameterization and the local reparameterization tricks, showing that, the computational complexity is reduced from $\mathcal{O}(D^2)$ to $\mathcal{O}(D \log D)$. Finally, unlike mean field VI, WHVI induces a matrix-variate distribution to approximate the posterior over the weights, thus increasing flexibility at a log-linear cost in D instead of linear.

We can think of our proposal as a specific factorization of the weight matrix, so we can speculate that other tensor factorizations [45] of the weight matrix could equally yield such benefits. Our comparison against various matrix factorization alternatives, however, shows that WHVI is superior to other parameterizations that have the same complexity. Furthermore, while matrix-variate posterior approximations have been proposed in the literature of VI [34], this comes at the expense of increasing the complexity, while our proposal keeps the complexity to log-linear in D .

Through a wide range of experiments on DNNs and CNNs, we demonstrate that our approach enables the possibility to run variational inference on complex over-parameterized models, while being competitive with state-of-the-art alternatives. Ultimately, our proposal shows how advances in kernel methods can be instrumental in improving VI, much like previous works showed how kernel methods can improve, e.g., Markov chain Monte Carlo sampling [51, 55] and statistical testing [19, 20, 65].

2 Walsh-Hadamard Variational Inference

2.1 Background on Structured Approximations of Kernel Matrices

WHVI is inspired by a line of works that developed from random feature expansions for kernel machines [48], which we briefly review here. A positive-definite kernel function $\kappa(\mathbf{x}_i, \mathbf{x}_j)$ induces a mapping $\phi(\mathbf{x})$, which can be infinite dimensional depending on the choice of $\kappa(\cdot, \cdot)$. Among the large literature of scalable kernel machines, random feature expansion techniques aim at constructing a finite approximation to $\phi(\cdot)$. For many kernel functions [48, 6], this approximation is built by applying a nonlinear transformation to a random projection $\mathbf{X}\mathbf{\Omega}$, where $\mathbf{\Omega}$ has entries $\mathcal{N}(\omega_{ij}|0, 1)$. If the matrix of training points \mathbf{X} is $N \times D$ and we are aiming to construct D random features, that is $\mathbf{\Omega}$ is $D \times D$, this requires N times $\mathcal{O}(D^2)$ time, which can be prohibitive when D is large.

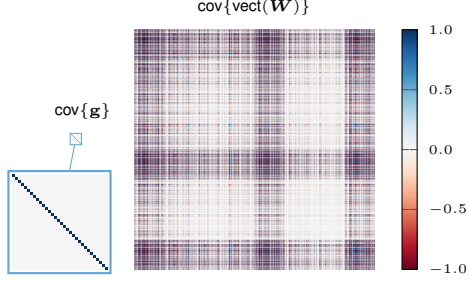


Figure 1: Normalized covariance of \mathbf{g} and $\text{vect}(\mathbf{W})$.

Table 1: Complexity of various approaches to VI

	COMPLEXITY	
	SPACE	TIME
MEAN FIELD GAUSSIAN	$\mathcal{O}(D^2)$	$\mathcal{O}(D^2)$
GAUSSIAN MATRIX VARIATE	$\mathcal{O}(D^2)$	$\mathcal{O}(D^2 + M^3)$
TENSOR FACTORIZATION	$\mathcal{O}(KR^2)$	$\mathcal{O}(R^2)$
WHVI	$\mathcal{O}(D)$	$\mathcal{O}(D \log D)$

Note: D is the dimensionality of the feature map, K is the number of tensor cores, R is the rank of tensor cores and M is the number of pseudo-data used to sample from a matrix Gaussian distribution (see [34]).

FASTFOOD [33] tackles the issue of large dimensional problems by replacing the matrix Ω with a random matrix for which the space complexity is reduced from $\mathcal{O}(D^2)$ to $\mathcal{O}(D)$ and time complexity of performing products with input vectors is reduced from $\mathcal{O}(D^2)$ to $\mathcal{O}(D \log D)$. In FASTFOOD, the matrix Ω is replaced by $\Omega \approx \mathbf{S} \mathbf{H} \mathbf{G} \mathbf{\Pi} \mathbf{H} \mathbf{B}$, where $\mathbf{\Pi}$ is a permutation matrix, \mathbf{H} is the Walsh-Hadamard matrix, whereas \mathbf{G} and \mathbf{B} are diagonal random matrices with standard Normal and Rademacher ($\{\pm 1\}$) distributions, respectively. The Walsh-Hadamard matrix is defined recursively starting from $H_2 = \begin{bmatrix} 1 & 1 \\ 1 & -1 \end{bmatrix}$ and then $H_{2D} = \begin{bmatrix} H_D & H_D \\ H_D & -H_D \end{bmatrix}$, possibly scaled by $D^{-1/2}$ to make it orthonormal. The product $\mathbf{H}\mathbf{x}$ can be computed in $\mathcal{O}(D \log D)$ time and $\mathcal{O}(1)$ space using the in-place version of the Fast Walsh-Hadamard Transform [FWHT, 13]. \mathbf{S} is also diagonal with i.i.d. entries, and it is chosen such that the elements of Ω obtained by this series of operations are approximately independent and follow a standard Normal (see [58] for more details). FASTFOOD inspired a series of other works on kernel approximations, whereby Gaussian random matrices are approximated by a series of products between diagonal Rademacher and Walsh-Hadamard matrices [64, 2].

2.2 From FASTFOOD to Walsh-Hadamard Variational Inference

FASTFOOD and its variants yield cheap approximations to Gaussian random matrices with pseudo-independent entries, and zero mean and unit variance. The question we address in this paper is whether we can use these types of approximations as cheap approximating distributions for VI. By considering a prior for the elements of the diagonal matrix $\mathbf{G} = \text{diag}(\mathbf{g})$ and a variational posterior $q(\mathbf{g}) = \mathcal{N}(\boldsymbol{\mu}, \boldsymbol{\Sigma})$, we can actually obtain a class of approximate posterior with some desirable properties as discussed next. Let $\mathbf{W} = \mathbf{W}^{(l)} \in \mathbb{R}^{D \times D}$ be the weight matrix of a DNN at layer (l) , and consider

$$\widetilde{\mathbf{W}} \sim q(\mathbf{W}) \quad \text{s.t.} \quad \widetilde{\mathbf{W}} = \mathbf{S}_1 \mathbf{H} \text{diag}(\widetilde{\mathbf{g}}) \mathbf{H} \mathbf{S}_2 \quad \text{with} \quad \widetilde{\mathbf{g}} \sim q(\mathbf{g}). \quad (2)$$

The choice of a Gaussian $q(\mathbf{g})$ and the linearity of the operations induce a parameterization of a matrix-variate Gaussian distribution for \mathbf{W} , which is controlled by \mathbf{S}_1 and \mathbf{S}_2 if we assume that we can optimize these diagonal matrices. Note that we have dropped the permutation matrix $\mathbf{\Pi}$ and we will show later that this is not critical for performance, while it speeds up computations.

For a generic $D_1 \times D_2$ matrix-variate Gaussian distribution, we have

$$\mathbf{W} \sim \mathcal{MN}(\mathbf{M}, \mathbf{U}, \mathbf{V}) \quad \text{if and only if} \quad \text{vect}(\mathbf{W}) \sim \mathcal{N}(\text{vect}(\mathbf{M}), \mathbf{V} \otimes \mathbf{U}), \quad (3)$$

where $\mathbf{M} \in \mathbb{R}^{D_1 \times D_2}$ is the mean matrix and $\mathbf{U} \in \mathbb{R}^{D_1 \times D_1}$ and $\mathbf{V} \in \mathbb{R}^{D_2 \times D_2}$ are two positive definite covariance matrices among rows and columns, and \otimes denotes the Kronecker product. In WHVI, as \mathbf{S}_2 is diagonal, $\mathbf{H} \mathbf{S}_2 = [\mathbf{v}_1, \dots, \mathbf{v}_D]$ with $\mathbf{v}_i = (\mathbf{S}_2)_{i,i} (\mathbf{H})_{:,i}$, so \mathbf{W} can be rewritten in terms of $\mathbf{A} \in \mathbb{R}^{D^2 \times D}$ and \mathbf{g} as follows

$$\text{vect}(\mathbf{W}) = \mathbf{A} \mathbf{g} \quad \text{where} \quad \mathbf{A}^\top = [(\mathbf{S}_1 \mathbf{H} \text{diag}(\mathbf{v}_1))^\top \dots (\mathbf{S}_1 \mathbf{H} \text{diag}(\mathbf{v}_D))^\top]. \quad (4)$$

This rewriting, shows that the choice of $q(\mathbf{g})$ yields $q(\text{vect}(\mathbf{W})) = \mathcal{N}(\mathbf{A} \boldsymbol{\mu}, \mathbf{A} \boldsymbol{\Sigma} \mathbf{A}^\top)$, proving that WHVI assumes a matrix-variate distribution $q(\mathbf{W})$, see Fig. 1 for an illustration of this.

We report the expression for M , U , and V and leave the full derivation to the Supplement. For the mean, we have $M = S_1 H \text{diag}(\mu) H S_2$, whereas for U and V , we have:

$$U^{1/2} = S_1 H T_2 \quad \text{and} \quad V^{1/2} = \frac{1}{\sqrt{\text{Tr}(U)}} S_2 H T_1, \quad (5)$$

where each row i of $T_1 \in \mathbb{R}^{D \times D^2}$ is the column-wise vectorization of $(\Sigma_{i,j}^{1/2} (H S_1)_{i,j'})_{j,j' \leq D}$, the matrix T_2 is defined similarly with S_2 instead of S_1 , and $\text{Tr}(\cdot)$ denotes the trace operator.

The mean of the structured matrix-variate posterior assumed by WHVI can span a D -dimensional linear subspace within the whole D^2 -dimensional parameter space, and the orientation is controlled by the matrices S_1 and S_2 ; more details on this geometric interpretation of WHVI can be found in the Supplement.

Matrix-variate Gaussian posteriors for variational inference have been introduced in [34]; however, assuming full covariance matrices U and V is memory and computationally intensive (quadratic and cubic in D , respectively). WHVI captures covariances across weights (see Fig. 1), while keeping memory requirements linear in D and complexity log-linear in D .

2.3 Reparameterizations in WHVI for Stochastic Optimization

The so-called *reparameterization trick* [28] is a standard way to make the variational lower bound in Eq. 1 a deterministic function of the variational parameters, so as to be able to carry out gradient-based optimization despite the stochasticity of the objective. Considering input vectors \mathbf{h}_i to a given layer, an improvement over this approach is to consider the distribution of the product $\mathbf{W} \mathbf{h}_i$. This is also known as the *local reparameterization trick* [29], and it reduces the variance of stochastic gradients in the optimization, thus improving convergence. The product $\mathbf{W} \mathbf{h}_i$ follows the distribution $\mathcal{N}(\mathbf{m}, \mathbf{A} \mathbf{A}^\top)$ [21], with

$$\mathbf{m} = S_1 H \text{diag}(\mu) H S_2 \mathbf{h}_i, \quad \text{and} \quad \mathbf{A} = S_1 H \text{diag}(H S_2 \mathbf{h}_i) \Sigma^{1/2}. \quad (6)$$

A sample from this distribution can be efficiently computed thanks to the Walsh-Hadamard transform as: $\overline{\mathbf{W}}(\mu) \mathbf{h}_i + \overline{\mathbf{W}}(\Sigma^{1/2} \epsilon) \mathbf{h}_i$, with $\overline{\mathbf{W}}$ a linear matrix-valued function $\overline{\mathbf{W}}(\mathbf{u}) = S_1 H \text{diag}(\mathbf{u}) H S_2$.

2.4 Alternative Structures and Comparison with Tensor Factorization

The choice of the parameterization of \mathbf{W} in WHVI leaves space to several possible alternatives, which we compare in Table 2. For all of them, \mathbf{G} is learned variationally and the remaining diagonal \mathbf{S}_i (if any) are either optimized or treated variationally (Gaussian mean-field). Fig. 2 shows the behavior of these alternatives when applied to a 2×64 network with ReLU activations. With the exception of the simple and highly constrained alternative \mathbf{GH} , all parameterizations are converging quite easily and the comparison with MCD shows that indeed the proposed WHVI performs better both in terms of ERROR RATE and MNLL. WHVI is effectively imposing a factorization of \mathbf{W} , where parameters are either optimized or treated variationally. Tensor decompositions for DNNs and CNNs have been proposed in [45]; here \mathbf{W} is decomposed into k small matrices (tensor cores), such that $\mathbf{W} = \mathbf{W}_1 \mathbf{W}_2 \cdots \mathbf{W}_k$, where each \mathbf{W}_i has dimensions $r_{i-1} \times r_i$ (with $r_1 = r_k = D$). We adapt this idea to make a comparison with WHVI. In order to match the space and time complexity of WHVI, assuming $\{r_i = R | \forall i = 2, \dots, k-1\}$, we set: $R \propto \log_2 D$ and $K \propto \frac{D}{(\log_2 D)^2}$. Also, to

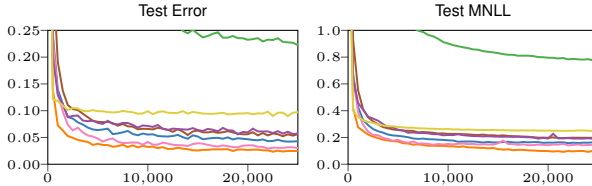


Figure 2: Ablation study of different structures for the parameterization of the weights distribution. Metric: test ERROR RATE and test MNLL with different structures for the weights. Benchmark on DRIVE with a 2×64 network.

Table 2: List of alternative structures and test performance on DRIVE dataset.

MODEL	TEST	
	ERROR	MNLL
MCD	0.097	0.249
\mathbf{GH}	0.226	0.773
$\mathbf{S}_{\text{var}} \mathbf{HGH}$	0.043	0.159
$\mathbf{S}_{1,\text{var}} \mathbf{HGH} \mathbf{S}_{2,\text{var}} \mathbf{H}$	0.061	0.190
$\mathbf{S}_{\text{opt}} \mathbf{HGH}$	0.054	0.199
$\mathbf{S}_{1,\text{opt}} \mathbf{HGH} \mathbf{S}_{2,\text{opt}} \mathbf{H}$	0.031	0.146
$\mathbf{S}_{1,\text{opt}} \mathbf{HGH} \mathbf{S}_{2,\text{opt}}$ (WHVI)	0.026	0.094

Colors are coded to match the ones used in the adjacent Figure

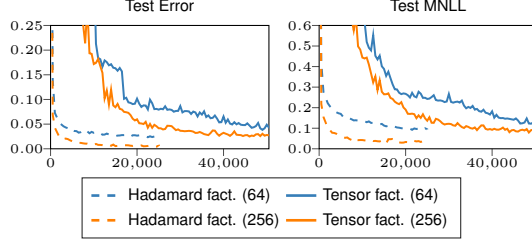


Figure 3: Comparison between Hadamard factorization in WHVI and tensor factorization. The number in the parenthesis is the hidden dimension. Plot is w.r.t. iterations rather than time to avoid implementation artifacts. The dataset used is DRIVE.

Algorithm 1: Setup dimensions for non-squared matrix

```

Function SetupDimensions( $D_{\text{in}}, D_{\text{out}}$ ):
    next power  $\leftarrow 2^{\lceil \log_2 D_{\text{in}} \rceil}$ ;
    if next power ==  $2D_{\text{in}}$  then
        padding  $\leftarrow 0$ ;
    else
        padding = next power -  $D_{\text{in}}$ ;
         $D_{\text{in}} \leftarrow$  next power;
    stack, remainder = divmod( $D_{\text{out}}, D_{\text{in}}$ );
    if remainder != 0 then
        stack  $\leftarrow$  stack + 1;
         $D_{\text{out}} \leftarrow D_{\text{in}} \times$  stack;
    return  $D_{\text{in}}, D_{\text{out}}, \text{padding}, \text{stack}$ 

```

match the number of variational parameters, all internal cores ($i = 2, \dots, k-1$) are learned with fully factorized Gaussian posterior, while the remaining are optimized (see Table 1). Given the same asymptotic complexity, Fig. 3 reports the results of this comparison again on a 2 hidden layer network. Not only WHVI can reach better solutions in terms of test performance, but optimization is also faster. We speculate that this is attributed to the redundant variational parameterization induced by the tensor cores, which makes the optimization landscapes highly multi-modal, leading to slow convergence.

2.5 Extensions

Concatenating or Reshaping Parameters for WHVI For the sake of presentation, so far we have assumed $\mathbf{W} \in \mathbb{R}^{D \times D}$ with $D = 2^d$, but we can easily extend WHVI to handle parameters of any shape $\mathbf{W} \in \mathbb{R}^{D_{\text{out}} \times D_{\text{in}}}$. One possibility is to use WHVI with a large $D \times D$ matrix with $D = 2^d$, such that a subset of its elements represent \mathbf{W} . Alternatively, a suitable value of d can be chosen so that \mathbf{W} is a concatenation by row/column of square matrices of size $D = 2^d$, padding if necessary (Algorithm 1 shows this case).

When one of the dimensions is equal to one so that the parameter matrix is a vector ($\mathbf{W} = \mathbf{w} \in \mathbb{R}^D$), this latter approach is not ideal, as WHVI would fall back on mean-field VI. WHVI can be extended to handle these cases efficiently by reshaping the parameter vector into a matrix of size 2^d with suitable d , again by padding if necessary. Thanks to the reshaping, WHVI uses \sqrt{D} parameters to model a posterior over D , and allows for computations in $\mathcal{O}(\sqrt{D} \log D)$ rather than D . This is possible by reshaping the vector that multiplies the weights in a similar way. In the Supplement, we explore this idea to infer parameters of Gaussian processes linearized using large numbers of random features.

Normalizing Flows Normalizing flows [NF, 49] are a family of parameterized distributions that allow for flexible approximations. In the general setting, consider a set of invertible, continuous and differentiable functions $f_k : \mathbb{R}^D \rightarrow \mathbb{R}^D$ with parameters λ_k . Given $\mathbf{z}_0 \sim q_0(\mathbf{z}_0)$, \mathbf{z}_0 is transformed with a chain of K flows to $\mathbf{z}_K = (f_K \circ \dots \circ f_1)(\mathbf{z}_0)$. The variational lower bound slightly differs from Eq. 1 to take into account the determinant of the Jacobian of the transformation, yielding a new variational objective as follows:

$$\mathbb{E}_{q_0} [\log p(\mathbf{Y}|\mathbf{X}, \mathbf{W})] - \text{KL}\{q_0(\mathbf{z}_0) || p(\mathbf{z}_K)\} + \mathbb{E}_{q_0(\mathbf{z}_0)} \left[\sum_{k=1}^K \log \left| \det \frac{\partial f_k(\mathbf{z}_{k-1}; \lambda_k)}{\partial \mathbf{z}_{k-1}} \right| \right]. \quad (7)$$

Setting the initial distribution q_0 to a fully factorized Gaussian $\mathcal{N}(\mathbf{z}_0 | \boldsymbol{\mu}, \boldsymbol{\sigma} \mathbf{I})$ and assuming a Gaussian prior on the generated \mathbf{z}_K , the KL term is analytically tractable. The transformation f is generally chosen to allow for fast computation of the determinant of the Jacobian. The parameters of the initial density q_0 as well as the flow parameters λ are optimized. In our case, we consider q_K as a distribution over the elements of \mathbf{g} . This approach increases the flexibility of the form of the variational posterior in WHVI, which is no longer Gaussian, while still capturing covariances across weights. This is obtained at the expense of losing the possibility of employing the local reparameterization trick. In the following Section, we will use *planar flows* [49]. Although this is a simple flow parameterization, a planar flow requires only $\mathcal{O}(D)$ parameters and thus it does not increase the time/space complexity of WHVI. More complex alternatives can be found in [59, 30, 35].

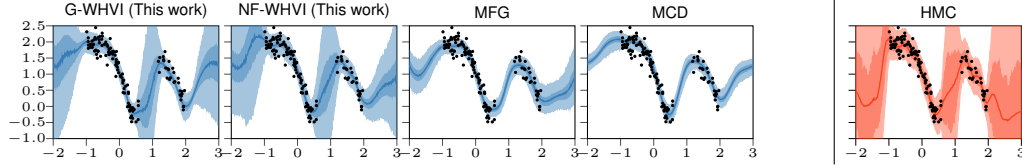


Figure 4: Regression example trained using WHVI with Gaussian vector (1541 param.) and with planar normalizing flow (10 flows for a total of 4141 param.), MFG (35k param.) and Monte Carlo dropout (MCD) (17k param.). The two shaded areas represent the 95th and the 75th percentile of the predictions. As “ground truth”, we also show the predictive posterior obtained by running SGHMC on the same model ($R < 1.05$, [17]).

3 Experiments

In this Section we will provide experimental evaluations of our proposal, with experiments ranging from regression on classic benchmark datasets to image classification with large-scale convolutional neural networks. We will also comment on the computational efficiency and some potential limitation of our proposal.

3.1 Toy example

We begin our experimental validation with a 1D-regression problem. We generated a 1D toy regression problem with 128 inputs sampled from $\mathcal{U}[-1, 2]$, and removed 20% inputs on a predefined interval; targets are noisy realizations of a random function (noise variance $\sigma^2 = \exp(-3)$). We model these data using a DNN with 2 hidden layers of 128 features and cosine activations. We test four models: mean-field Gaussian VI (MFG), Monte Carlo dropout [MCD, 15] with dropout rate 0.4 and two variants of WHVI – G-WHVI with Gaussian posterior and NF-WHVI with planar flows (10 planar flows). We also show the free form posterior obtained by running a MCMC algorithm, SGHMC in this case [5, 54], for several thousands steps. As Fig. 4 shows, WHVI offers a sensible modeling of the uncertainty on the input domain, whereas MFG and MCD seem to be slightly over-confident.

3.2 Bayesian Neural Networks

We conduct a series of comparisons with state-of-the-art VI schemes for Bayesian DNNs; see the Supplement for the list of data sets used in the experiments. We compare WHVI with MCD and NNG [NOISY-KFAC, 66]. MCD draws on a formal connection between dropout and VI with Bernoulli-like posteriors, while the more recent NOISY-KFAC yields a matrix-variate Gaussian distribution using noisy natural gradients. To these baselines, we also add the comparison with mean field Gaussian (MFG). In WHVI, the last layer assumes a fully factorized Gaussian posterior.

Data is randomly divided into 90%/10% splits for training and testing eight times. We standardize the input features \mathbf{x} while keeping the targets \mathbf{y} unnormalized. Differently from the experimental setup in [34, 66, 23], we use the same architecture regardless of the size of the dataset. Furthermore, to test the efficiency of WHVI in case of over-parameterized models, we set the network to have two hidden layers and 128 features with ReLU activations (as a reference, these models are ~ 20 times bigger than the usual setup, which uses a single hidden layer with 50/100 units).

We report the test RMSE and the average predictive test negative log-likelihood (MNLL) in Table 3. On the majority of the datasets, WHVI outperforms MCD and NOISY-KFAC.

Table 3: Test RMSE and test MNLL for regression datasets. Results in the format “mean (std)”

MODEL DATASET	TEST ERROR				TEST MNLL			
	MCD	MFG	NNG	WHVI	MCD	MFG	NNG	WHVI
BOSTON	3.91 (0.86)	4.47 (0.85)	3.56 (0.43)	3.14 (0.71)	6.90 (2.93)	2.99 (0.41)	2.72 (0.09)	4.33 (1.80)
CONCRETE	5.12 (0.79)	8.01 (0.41)	8.21 (0.55)	4.70 (0.72)	3.20 (0.36)	3.41 (0.05)	3.56 (0.08)	3.17 (0.37)
ENERGY	2.07 (0.11)	3.10 (0.14)	1.96 (0.28)	0.58 (0.07)	4.15 (0.15)	4.91 (0.09)	2.11 (0.12)	2.00 (0.60)
KIN8NM	0.09 (0.00)	0.12 (0.00)	0.07 (0.00)	0.08 (0.00)	-0.87 (0.02)	-0.83 (0.02)	-1.19 (0.04)	-1.19 (0.04)
NAVAL	0.30 (0.30)	0.01 (0.00)	0.00 (0.00)	0.01 (0.00)	-1.00 (2.27)	-6.23 (0.01)	-6.52 (0.09)	-6.25 (0.01)
POWERPLANT	3.97 (0.14)	4.52 (0.13)	4.23 (0.09)	4.00 (0.12)	2.74 (0.05)	2.83 (0.03)	2.86 (0.02)	2.71 (0.03)
PROTEIN	4.23 (0.10)	4.93 (0.11)	4.57 (0.47)	4.36 (0.11)	2.76 (0.02)	2.92 (0.01)	2.95 (0.12)	2.79 (0.01)
YACHT	1.90 (0.54)	7.01 (1.22)	5.16 (1.48)	0.69 (0.16)	2.95 (1.27)	3.38 (0.29)	3.06 (0.27)	1.80 (1.01)

Furthermore, we study how the test MNLL varies with the number of hidden units in a 2-layered network. As Fig. 5 shows, WHVI behaves well while competitive methods struggle. Empirically, these results demonstrate the value of WHVI, which offers a competitive parameterization of a matrix-variate Gaussian posterior while requiring log-linear time in D . We refer the Reader to the Supplement for additional details on the experimental setup and for the benchmark with the classic architectures.

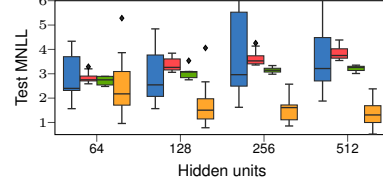


Figure 5: Comparison of the test MNLL as a function of the number of hidden units for MCD (●), MFG (●), NNG (●) and WHVI (●). The dataset used is YACHT.

3.3 Bayesian Convolutional Neural Networks

We continue the experimental evaluation of WHVI by analyzing its performance on CNNs. For this experiment, we replace all fully-connected layers in the CNN with the WHVI parameterization, while the convolutional filters are treated variationally using MCD. In this setup, we fit VGG16 [52], ALEXNET [31] and RESNET-18 [22] on CIFAR10. Using WHVI, we can reduce the number of parameters in the linear layers without affecting neither test performance nor calibration properties of the resulting model, as shown in Fig. 6 and Table 4. For ALEXNET and RESNET we also try our variant of WHVI with NF. Even though we lose the benefits of the local reparameterization, the higher flexibility of normalizing flows allows the model to obtain better test performance with respect to the Gaussian posterior. This can be improved even further using more complex families of normalizing flows [49, 59, 30, 35]. With WHVI, ALEXNET and its original $\sim 23.3\text{M}$ parameters is reduced to just $\sim 2.3\text{M}$ (9.9%) when using G-WHVI and to $\sim 2.4\text{M}$ (10.2%) with WHVI and 3 planar flows.

WHVI for convolutional filters By observing that the convolution can be written as matrix multiplication (once filters are reshaped in 2D), we also extended WHVI for convolutional layers.

We observe though that in this case resulting models had too few parameters to obtain any interesting results. For ALEXNET, we obtained a model with just 189K parameters, which corresponds to a sparsity of 99.2% with respect of the original model. As a reference, Wen et al. [60] was able to reach sparsity only up to 60% in the convolutional layers without impacting performance.

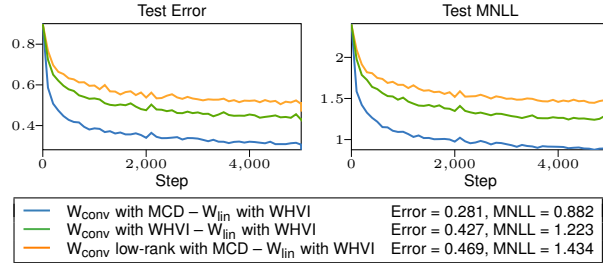


Figure 7: Inference of convolutional filters (dataset: CIFAR10).

To study this behavior in details, we take a simple CNN with two convolutional layers and one linear layer (Fig. 7). We see that the combination of MCD and WHVI performs very well in terms of convergence and test performance, while the use of WHVI on the convolutional filters brings an overall degradation of the performance. Interestingly, though, we also observe that MCD with the same number of parameters as for WHVI (referred to as low-rank MCD) performs even worse than the baseline: this once again confirms the parameterization of WHVI as an efficient alternative.

Table 4: Test performance of different Bayesian CNNs.

	CIFAR10	TEST ERROR	TEST MNLL
VGG16	MFG	16.82%	0.6443
	MCD	21.47%	0.8213
	NNG	15.21%	0.6374
	WHVI	12.85%	0.6995
ALEXNET	MCD	13.30%	0.9590
	NNG	20.36%	—
	WHVI	13.56%	0.6164
	NF-WHVI	12.72%	0.6596
RESNET18	MCD	10.71%	0.8468
	NNG	—	—
	WHVI	11.46%	0.5513
	NF-WHVI	11.42%	0.4908

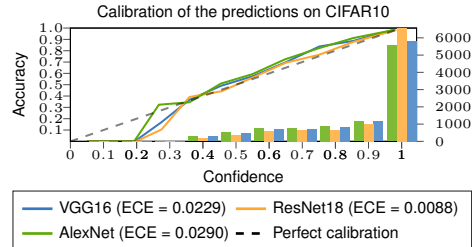


Figure 6: Reliability diagram and expected calibration error (ECE) of VGG16, ALEXNET and RESNET with WHVI [9, 44, 40].

3.4 Comments on computational efficiency

WHVI builds his computational efficiency on the Fast Walsh-Hadamard Transform (FWHT), which allows one to cut the complexity of a D -dimensional matrix-vector multiplication from a naive $\mathcal{O}(D^2)$ to $\mathcal{O}(D \log D)$. To empirically validate this claim, we extended PYTORCH [47] with a custom C++/CUDA kernel which implements a batched-version of the FWHT. The workstation used is equipped with two Intel Xeon CPUs, four NVIDIA Tesla P100 and 512 GB of RAM. Each experiment is carried out on a GPU fully dedicated to it. The NNG algorithm is implemented in TENSORFLOW² while the others are written in PYTORCH.

We made sure to fully exploit all parallelization opportunities in the competing methods and ours; we believe that the timings are not severely affected by external factors other than the actual implementation of the algorithms. The box-plots in Fig. 16 report the time required to sample and infer the carry out inference on the test set on two regression datasets as a function of the number of hidden units in a two-layer DNN. We speculate that the poor performance of NNG is due to the inversion of the approximation to the Fisher matrix, which scales cubically in the number of units.

Similar behavior can also be observed for Bayesian CNNs. In Fig. 9, we analyze the energy consumption required to sample from the converged model and predict on the test set of CIFAR10 with ALEXNET using WHVI and MCD. The regularity of the algorithm for computing the FWHT and its reduced memory footprint result on an overall higher utilization of the GPU, 85% for WHVI versus $\sim 70\%$ for MCD. This translates into an increase of energy efficiency up to 33% w.r.t MCD, despite being 51% faster.

Additional results and insights We refer the reader to the Supplement for an extended version of the results, including new applications of WHVI to GPUs.

Related Work

In the early sections of the paper, we have already briefly reviewed some of the literature on VI and Bayesian DNNs and CNNs; here we complement the literature by including other relevant works that have connections with WHVI.

Our work takes inspiration from the works on random features for kernel approximation [48] and FASTFOOD [33]. Random feature expansions have had a wide impact on the literature on kernel methods. Such approximations have been successfully used to scale a variety of models, such as Support Vector Machines [48], Gaussian processes [32] and Deep Gaussian processes [7, 15]. This has contributed to bridging the gap between Deep GPs and Bayesian DNNs and CNNs [41, 12, 7, 14], which is an active area of research which aims to gain a better understanding of deep learning models through the use of kernel methods [8, 11, 16]. Structured random features [33, 64, 2] have been also applied to the problem of handling large dimensional convolutional features [63] and Convolutional GPs [57].

Bayesian inference on DNNs and CNNs has been research topic of several seminar works [see e.g. 18, 23, 1, 15, 14]. Recent advances in DNNs have investigated the effect of over-parameterization and how model compression can be used during or after training [25, 36, 67]. Our current understanding shows that model performance is affected by the network size with bigger and wider neural networks

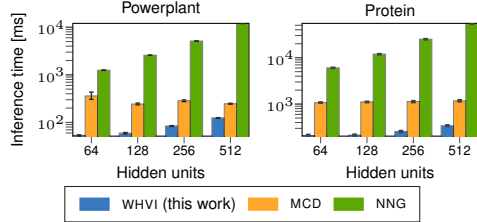


Figure 8: Inference time on the test set with 128 batch size and 64 Monte Carlo samples. Experiment repeated 100 times. Additional datasets available in the Supplement.

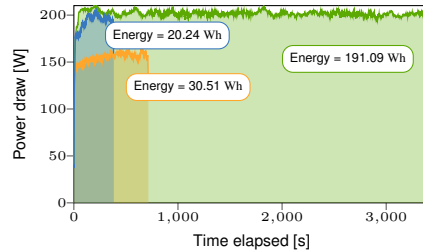


Figure 9: Power profiling during inference on the test set of CIFAR10 with ALEXNET and WHVI (●), MCD (●) and NNG (●). The task is repeated 16 consecutive times and profiling is carried out using the `nvidia-smi` tool.

¹github.com/gd-zhang/noisy-K-FAC — github.com/pomonam/NoisyNaturalGradient

being more resilient to overfit [42, 43]. For variational inference, and Bayesian inference in general, over-parameterization is reflected on over-regularization of the objective, leading the optimization to converge to trivial solutions (posterior equal to prior). Several works have encountered and proposed solutions to such issue [24, 4, 3, 53, 50]. The problem of how to run accurate Bayesian inference on over-parametrized models like BNN is still an ongoing open question [62, 61]

4 Conclusions

Inspired by the literature on scalable kernel methods, this paper proposed Walsh-Hadamard Variational Inference (WHVI). WHVI offers a novel parameterization of the variational posterior, which is particularly attractive for over-parameterized models, such as modern DNNs and CNNs. WHVI assumes a matrix-variate posterior distribution, which therefore captures covariances across weights. Crucially, unlike previous work on matrix-variate posteriors for VI, this is achieved with a light parameterization and fast computations, bypassing the over-regularization issues of VI for over-parameterized models. The large experimental campaign, demonstrates that WHVI is a strong competitor of other variational approaches for such models, while offering considerable speedups.

We are currently investigating other extensions where we capture the covariance between weights across layers, by either sharing the matrix G across, or by concatenating all weights into a single matrix which is then treated using WHVI, with the necessary adaptations to handle the sequential nature of computations. Finally, we are looking into deriving error bounds when using WHVI to approximate a generic matrix distribution; as preliminary work, in a numerical study in the supplement we show that the weights induced by WHVI can approximate reasonably well any arbitrary weight matrix, showing a consistent behavior w.r.t. increasing dimensions D .

Broader Impact

Bayesian inference for Deep Neural Networks (DNNs) and Convolutional Neural Networks (CNNs) offers attractive solutions to many problems where one needs to combine the flexibility of these deep models with the possibility to accurately quantify uncertainty in predictions and model parameters. This is of fundamental importance in an increasingly large number of applications of machine learning in society where uncertainty matters, and where calibration of the predictions and resilience to adversarial attacks are desirable.

Due to the intractability of Bayesian inference for such models, one needs to resort to approximations. Variational inference (VI) gained popularity before long the deep learning revolution, which has seen a considerable interest in the application of VI to DNNs and CNNs in the last decade. However, VI is still under appreciated in the deep learning community because it comes with a higher computational cost for optimization, sampling, storage and inference. With this work, we offer a novel solution to this problem to make VI truly scalable in each of its parts (parameterization, sampling and inference).

Our approach is inspired by the literature on kernel methods, and we believe that this cross-fertilization will enable further contributions in both communities. In the long term, our work will make it possible to accelerate training/inference of Bayesian deep models, while reducing their storage requirements. This will complement Bayesian compression techniques to facilitate the deployment of Bayesian deep models onto FPGA, ASIC and embedded processors.

Acknowledgments and Disclosure of Funding

The Authors would like to thanks Dino Sejdinovic for the insightful discussion on tensor decomposition, which resulted in the comparison in § 2.4. SR would like to thank Pietro Michiardi for allocating significant resources to our experimental campaign on the Zoe cloud computing platform [46]. MF gratefully acknowledges support from the AXA Research Fund and the Agence Nationale de la Recherche (grant ANR-18-CE46-0002).

References

- [1] C. Blundell, J. Cornebise, K. Kavukcuoglu, and D. Wierstra. Weight Uncertainty in Neural Network. In F. Bach and D. Blei, editors, *Proceedings of the 32nd International Conference on*

- Machine Learning*, volume 37 of *Proceedings of Machine Learning Research*, pages 1613–1622, Lille, France, 07–09 Jul 2015. PMLR.
- [2] M. Bojarski, A. Choromanska, K. Choromanski, F. Fagan, C. Gouy-Pailler, A. Morvan, N. Sakr, T. Sarlos, and J. Atif. Structured Adaptive and Random Spinners for Fast Machine Learning Computations. In A. Singh and J. Zhu, editors, *Proceedings of the 20th International Conference on Artificial Intelligence and Statistics*, volume 54 of *Proceedings of Machine Learning Research*, pages 1020–1029, Fort Lauderdale, FL, USA, 20–22 Apr 2017. PMLR.
 - [3] S. R. Bowman, L. Vilnis, O. Vinyals, A. Dai, R. Jozefowicz, and S. Bengio. Generating Sentences from a Continuous Space. In *Proceedings of The 20th SIGNLL Conference on Computational Natural Language Learning*, pages 10–21. Association for Computational Linguistics, 2016.
 - [4] C. P. Burgess, I. Higgins, A. Pal, L. Matthey, N. Watters, G. Desjardins, and A. Lerchner. Understanding disentangling in β -VAE. *CoRR*, abs/1804.03599, 2018.
 - [5] T. Chen, E. Fox, and C. Guestrin. Stochastic Gradient Hamiltonian Monte Carlo. In E. P. Xing and T. Jebara, editors, *Proceedings of the 31st International Conference on Machine Learning*, *Proceedings of Machine Learning Research*, pages 1683–1691, Beijing, China, 22–24 Jun 2014. PMLR.
 - [6] Y. Cho and L. K. Saul. Kernel Methods for Deep Learning. In Y. Bengio, D. Schuurmans, J. D. Lafferty, C. K. I. Williams, and A. Culotta, editors, *Advances in Neural Information Processing Systems 22*, pages 342–350. Curran Associates, Inc., 2009.
 - [7] K. Cutajar, E. V. Bonilla, P. Michiardi, and M. Filippone. Random feature expansions for deep Gaussian processes. In D. Precup and Y. W. Teh, editors, *Proceedings of the 34th International Conference on Machine Learning*, volume 70 of *Proceedings of Machine Learning Research*, pages 884–893, International Convention Centre, Sydney, Australia, Aug. 2017. PMLR.
 - [8] A. G. de G. Matthews, J. Hron, M. Rowland, R. E. Turner, and Z. Ghahramani. Gaussian Process Behaviour in Wide Deep Neural Networks. In *International Conference on Learning Representations*, 2018.
 - [9] M. H. DeGroot and S. E. Fienberg. The comparison and evaluation of forecasters. *Journal of the Royal Statistical Society. Series D (The Statistician)*, 32(1/2):12–22, 1983. ISSN 00390526, 14679884.
 - [10] S. Ding and D. Cook. Dimension folding PCA and PFC for matrix-valued predictors. *Statistica Sinica*, 24(1):463–492, 2014.
 - [11] M. M. Dunlop, M. A. Girolami, A. M. Stuart, and A. L. Teckentrup. How Deep Are Deep Gaussian Processes? *Journal of Machine Learning Research*, 19(1):2100–2145, Jan. 2018. ISSN 1532-4435.
 - [12] D. K. Duvenaud, O. Rippel, R. P. Adams, and Z. Ghahramani. Avoiding pathologies in very deep networks. In *Proceedings of the Seventeenth International Conference on Artificial Intelligence and Statistics, AISTATS 2014, Reykjavik, Iceland, April 22-25, 2014*, volume 33 of *JMLR Workshop and Conference Proceedings*, pages 202–210. JMLR.org, 2014.
 - [13] Fino and Algazi. Unified Matrix Treatment of the Fast Walsh-Hadamard Transform. *IEEE Transactions on Computers*, C-25(11):1142–1146, Nov 1976. ISSN 0018-9340.
 - [14] Y. Gal and Z. Ghahramani. Bayesian Convolutional Neural Networks with Bernoulli Approximate Variational Inference. *CoRR*, abs/1506.02158, 2015.
 - [15] Y. Gal and Z. Ghahramani. Dropout As a Bayesian Approximation: Representing Model Uncertainty in Deep Learning. In *Proceedings of the 33rd International Conference on International Conference on Machine Learning - Volume 48, ICML’16*, pages 1050–1059. JMLR.org, 2016.
 - [16] A. Garriga-Alonso, C. E. Rasmussen, and L. Aitchison. Deep Convolutional Networks as shallow Gaussian Processes. In *International Conference on Learning Representations*, 2019.

- [17] A. Gelman, J. B. Carlin, H. S. Stern, and D. B. Rubin. *Bayesian Data Analysis*. Chapman and Hall/CRC, 2nd ed. edition, 2004.
- [18] A. Graves. Practical Variational Inference for Neural Networks. In J. Shawe-Taylor, R. S. Zemel, P. L. Bartlett, F. Pereira, and K. Q. Weinberger, editors, *Advances in Neural Information Processing Systems 24*, pages 2348–2356. Curran Associates, Inc., 2011.
- [19] A. Gretton, K. Fukumizu, C. H. Teo, L. Song, B. Schölkopf, and A. J. Smola. A Kernel Statistical Test of Independence. In J. C. Platt, D. Koller, Y. Singer, and S. T. Roweis, editors, *Advances in Neural Information Processing Systems 20*, pages 585–592. Curran Associates, Inc., 2008.
- [20] A. Gretton, K. M. Borgwardt, M. J. Rasch, B. Schölkopf, and A. Smola. A Kernel Two-sample Test. *Journal of Machine Learning Research*, 13:723–773, Mar. 2012. ISSN 1532-4435.
- [21] A. K. Gupta and D. K. Nagar. *Matrix variate distributions*. Chapman and Hall/CRC, 1999.
- [22] K. He, X. Zhang, S. Ren, and J. Sun. Deep Residual Learning for Image Recognition. In *2016 IEEE Conference on Computer Vision and Pattern Recognition, CVPR 2016, Las Vegas, NV, USA, June 27-30, 2016*, pages 770–778, 2016.
- [23] J. M. Hernandez-Lobato and R. Adams. Probabilistic backpropagation for scalable learning of bayesian neural networks. In F. Bach and D. Blei, editors, *Proceedings of the 32nd International Conference on Machine Learning*, volume 37 of *Proceedings of Machine Learning Research*, pages 1861–1869, Lille, France, 07–09 Jul 2015. PMLR.
- [24] I. Higgins, L. Matthey, A. Pal, C. Burgess, X. Glorot, M. Botvinick, S. Mohamed, and A. Lerchner. beta-VAE: Learning Basic Visual Concepts with a Constrained Variational Framework. In *International Conference on Learning Representations*, 2017.
- [25] I. Hubara, M. Courbariaux, D. Soudry, R. El-Yaniv, and Y. Bengio. Binarized neural networks. In D. D. Lee, M. Sugiyama, U. V. Luxburg, I. Guyon, and R. Garnett, editors, *Advances in Neural Information Processing Systems 29*, pages 4107–4115. Curran Associates, Inc., 2016.
- [26] M. I. Jordan, Z. Ghahramani, T. S. Jaakkola, and L. K. Saul. An Introduction to Variational Methods for Graphical Models. *Machine Learning*, 37(2):183–233, Nov. 1999.
- [27] D. P. Kingma and J. Ba. Adam: A Method for Stochastic Optimization. In *Proceedings of the Third International Conference on Learning Representations*, San Diego, USA, May 2015.
- [28] D. P. Kingma and M. Welling. Auto-Encoding Variational Bayes. In *Proceedings of the Second International Conference on Learning Representations (ICLR 2014)*, Apr. 2014.
- [29] D. P. Kingma, T. Salimans, and M. Welling. Variational Dropout and the Local Reparameterization Trick. In *Advances in Neural Information Processing Systems 28*, pages 2575–2583. Curran Associates, Inc., 2015.
- [30] D. P. Kingma, T. Salimans, R. Jozefowicz, X. Chen, I. Sutskever, and M. Welling. Improved Variational Inference with Inverse Autoregressive Flow. In D. D. Lee, M. Sugiyama, U. V. Luxburg, I. Guyon, and R. Garnett, editors, *Advances in Neural Information Processing Systems 29*, pages 4743–4751. Curran Associates, Inc., 2016.
- [31] A. Krizhevsky, I. Sutskever, and G. E. Hinton. ImageNet Classification with Deep Convolutional Neural Networks. In F. Pereira, C. J. C. Burges, L. Bottou, and K. Q. Weinberger, editors, *Advances in Neural Information Processing Systems 25*, pages 1097–1105. Curran Associates, Inc., 2012.
- [32] M. Lázaro-Gredilla, J. Quinonero-Candela, C. E. Rasmussen, and A. R. Figueiras-Vidal. Sparse Spectrum Gaussian Process Regression. *Journal of Machine Learning Research*, 11:1865–1881, 2010.
- [33] Q. Le, T. Sarlos, and A. Smola. Fastfood - Approximating Kernel Expansions in Loglinear Time. In *30th International Conference on Machine Learning (ICML)*, 2013.

- [34] C. Louizos and M. Welling. Structured and Efficient Variational Deep Learning with Matrix Gaussian Posteriors. In M. F. Balcan and K. Q. Weinberger, editors, *Proceedings of The 33rd International Conference on Machine Learning*, volume 48 of *Proceedings of Machine Learning Research*, pages 1708–1716, New York, New York, USA, 20–22 Jun 2016. PMLR.
- [35] C. Louizos and M. Welling. Multiplicative Normalizing Flows for Variational Bayesian Neural Networks. In D. Precup and Y. W. Teh, editors, *Proceedings of the 34th International Conference on Machine Learning*, volume 70 of *Proceedings of Machine Learning Research*, pages 2218–2227, International Convention Centre, Sydney, Australia, 06–11 Aug 2017. PMLR.
- [36] C. Louizos, K. Ullrich, and M. Welling. Bayesian Compression for Deep Learning. In I. Guyon, U. V. Luxburg, S. Bengio, H. Wallach, R. Fergus, S. Vishwanathan, and R. Garnett, editors, *Advances in Neural Information Processing Systems 30*, pages 3288–3298. Curran Associates, Inc., 2017.
- [37] D. J. C. Mackay. Bayesian methods for backpropagation networks. In E. Domany, J. L. van Hemmen, and K. Schulten, editors, *Models of Neural Networks III*, chapter 6, pages 211–254. Springer, 1994.
- [38] A. G. d. G. Matthews, M. van der Wilk, T. Nickson, K. Fujii, A. Boukouvalas, P. León-Villagrà, Z. Ghahramani, and J. Hensman. GPflow: A Gaussian process library using TensorFlow. *Journal of Machine Learning Research*, 18(40):1–6, apr 2017.
- [39] D. Molchanov, A. Ashukha, and D. Vetrov. Variational Dropout Sparsifies Deep Neural Networks. In D. Precup and Y. W. Teh, editors, *Proceedings of the 34th International Conference on Machine Learning*, volume 70 of *Proceedings of Machine Learning Research*, pages 2498–2507, International Convention Centre, Sydney, Australia, 06–11 Aug 2017. PMLR.
- [40] M. P. Naeini, G. F. Cooper, and M. Hauskrecht. Obtaining well calibrated probabilities using Bayesian binning. In *AAAI*, pages 2901–2907. AAAI Press, 2015.
- [41] R. M. Neal. *Bayesian Learning for Neural Networks*. Springer-Verlag, Berlin, Heidelberg, 1996. ISBN 0387947248.
- [42] B. Neyshabur, R. Tomioka, and N. Srebro. In Search of the Real Inductive Bias: On the Role of Implicit Regularization in Deep Learning. In *ICLR (Workshop)*, 2015.
- [43] B. Neyshabur, Z. Li, S. Bhojanapalli, Y. LeCun, and N. Srebro. The role of over-parametrization in generalization of neural networks. In *International Conference on Learning Representations*, 2019.
- [44] A. Niculescu-Mizil and R. Caruana. Predicting Good Probabilities with Supervised Learning. In *Proceedings of the 22Nd International Conference on Machine Learning*, ICML ’05, pages 625–632, New York, NY, USA, 2005. ACM.
- [45] A. Novikov, D. Podoprikin, A. Osokin, and D. P. Vetrov. Tensorizing Neural Networks. In C. Cortes, N. D. Lawrence, D. D. Lee, M. Sugiyama, and R. Garnett, editors, *Advances in Neural Information Processing Systems 28*, pages 442–450. Curran Associates, Inc., 2015.
- [46] F. Pace, D. Venzano, D. Carra, and P. Michiardi. Flexible scheduling of distributed analytic applications. In *Proceedings of the 17th IEEE/ACM International Symposium on Cluster, Cloud and Grid Computing (CCGRID ’17)*, pages 100–109, May 2017.
- [47] A. Paszke, S. Gross, S. Chintala, G. Chanan, E. Yang, Z. DeVito, Z. Lin, A. Desmaison, L. Antiga, and A. Lerer. Automatic differentiation in PyTorch. In *NIPS-W*, 2017.
- [48] A. Rahimi and B. Recht. Random Features for Large-Scale Kernel Machines. In J. C. Platt, D. Koller, Y. Singer, and S. T. Roweis, editors, *Advances in Neural Information Processing Systems 20*, pages 1177–1184. Curran Associates, Inc., 2008.
- [49] D. Rezende and S. Mohamed. Variational Inference with Normalizing Flows. In F. Bach and D. Blei, editors, *Proceedings of the 32nd International Conference on Machine Learning*, volume 37 of *Proceedings of Machine Learning Research*, pages 1530–1538, Lille, France, 07–09 Jul 2015. PMLR.

- [50] S. Rossi, P. Michiardi, and M. Filippone. Good Initializations of Variational Bayes for Deep Models. In K. Chaudhuri and R. Salakhutdinov, editors, *Proceedings of the 36th International Conference on Machine Learning*, volume 97 of *Proceedings of Machine Learning Research*, pages 5487–5497, Long Beach, California, USA, 09–15 Jun 2019. PMLR.
- [51] D. Sejdinovic, H. Strathmann, M. L. Garcia, C. Andrieu, and A. Gretton. Kernel Adaptive Metropolis-Hastings. In E. P. Xing and T. Jebara, editors, *Proceedings of the 31st International Conference on Machine Learning*, volume 32 of *Proceedings of Machine Learning Research*, pages 1665–1673, Beijing, China, 22–24 Jun 2014. PMLR.
- [52] K. Simonyan and A. Zisserman. Very Deep Convolutional Networks for Large-Scale Image Recognition. *CoRR*, abs/1409.1556, 2014.
- [53] C. K. Sønderby, T. Raiko, L. Maaløe, S. K. Sønderby, and O. Winther. Ladder Variational Autoencoders. In D. D. Lee, M. Sugiyama, U. V. Luxburg, I. Guyon, and R. Garnett, editors, *Advances in Neural Information Processing Systems 29*, pages 3738–3746. Curran Associates, Inc., 2016.
- [54] J. T. Springenberg, A. Klein, S. Falkner, and F. Hutter. Bayesian Optimization with Robust Bayesian Neural Networks. In D. D. Lee, M. Sugiyama, U. V. Luxburg, I. Guyon, and R. Garnett, editors, *Advances in Neural Information Processing Systems 29*, pages 4134–4142. Curran Associates, Inc., 2016.
- [55] H. Strathmann, D. Sejdinovic, S. Livingstone, Z. Szabo, and A. Gretton. Gradient-free Hamiltonian Monte Carlo with Efficient Kernel Exponential Families. In C. Cortes, N. D. Lawrence, D. D. Lee, M. Sugiyama, and R. Garnett, editors, *Advances in Neural Information Processing Systems 28*, pages 955–963. Curran Associates, Inc., 2015.
- [56] S. Surjanovic and D. Bingham. Virtual library of simulation experiments: Test functions and datasets. Retrieved May 22, 2019, from <http://www.sfu.ca/~ssurjano>.
- [57] G.-L. Tran, E. V. Bonilla, J. Cunningham, P. Michiardi, and M. Filippone. Calibrating Deep Convolutional Gaussian Processes. In K. Chaudhuri and M. Sugiyama, editors, *Proceedings of Machine Learning Research*, volume 89 of *Proceedings of Machine Learning Research*, pages 1554–1563. PMLR, 16–18 Apr 2019.
- [58] J. A. Tropp. Improved Analysis of the subsampled Randomized Hadamard Transform. *Advances in Adaptive Data Analysis*, 3(1-2):115–126, 2011.
- [59] R. Van den Berg, L. Hasenclever, J. M. Tomczak, and M. Welling. Sylvester Normalizing Flows for Variational Inference. In *UAI '18: Proceedings of the Thirty-Fourth Conference on Uncertainty in Artificial Intelligence*, 2018.
- [60] W. Wen, C. Wu, Y. Wang, Y. Chen, and H. Li. Learning Structured Sparsity in Deep Neural Networks. In D. D. Lee, M. Sugiyama, U. V. Luxburg, I. Guyon, and R. Garnett, editors, *Advances in Neural Information Processing Systems 29*, pages 2074–2082. Curran Associates, Inc., 2016.
- [61] F. Wenzel, K. Roth, B. S. Veeling, J. Świątkowski, L. Tran, S. Mandt, J. Snoek, T. Salimans, R. Jenatton, and S. Nowozin. How Good is the Bayes Posterior in Deep Neural Networks Really?, 2020.
- [62] A. G. Wilson and P. Izmailov. Bayesian Deep Learning and a Probabilistic Perspective of Generalization, 2020.
- [63] Z. Yang, M. Moczulski, M. Denil, N. d. Freitas, A. Smola, L. Song, and Z. Wang. Deep fried convnets. In *2015 IEEE International Conference on Computer Vision (ICCV)*, pages 1476–1483, Dec 2015.
- [64] F. X. Yu, A. T. Suresh, K. M. Choromanski, D. N. Holtmann-Rice, and S. Kumar. Orthogonal Random Features. In D. D. Lee, M. Sugiyama, U. V. Luxburg, I. Guyon, and R. Garnett, editors, *Advances in Neural Information Processing Systems 29*, pages 1975–1983. Curran Associates, Inc., 2016.

- [65] W. Zaremba, A. Gretton, and M. Blaschko. B-test: A Non-parametric, Low Variance Kernel Two-sample Test. In C. J. C. Burges, L. Bottou, M. Welling, Z. Ghahramani, and K. Q. Weinberger, editors, *Advances in Neural Information Processing Systems 26*, pages 755–763. Curran Associates, Inc., 2013.
- [66] G. Zhang, S. Sun, D. Duvenaud, and R. Grosse. Noisy Natural Gradient as Variational Inference. In J. Dy and A. Krause, editors, *Proceedings of the 35th International Conference on Machine Learning*, volume 80 of *Proceedings of Machine Learning Research*, pages 5852–5861, Stockholmsmässan, Stockholm Sweden, 10–15 Jul 2018. PMLR.
- [67] M. Zhu and S. Gupta. To Prune, or Not to Prune: Exploring the Efficacy of Pruning for Model Compression. In *ICLR (Workshop)*. OpenReview.net, 2018.

A Matrix-variate Posterior Distribution Induced by WHVI

We derive the parameters of the matrix-variate distribution $q(\mathbf{W}) = \mathcal{MN}(\mathbf{M}, \mathbf{U}, \mathbf{V})$ of the weight matrix $\mathbf{W} \in \mathbb{R}^{D \times D}$ given by WHVI,

$$\tilde{\mathbf{W}} = \mathbf{S}_1 \mathbf{H} \text{diag}(\tilde{\mathbf{g}}) \mathbf{H} \mathbf{S}_2 \quad \text{with} \quad \tilde{\mathbf{g}} \sim \mathcal{N}(\boldsymbol{\mu}, \boldsymbol{\Sigma}). \quad (8)$$

The mean $\mathbf{M} = \mathbf{S}_1 \mathbf{H} \text{diag}(\boldsymbol{\mu}) \mathbf{H} \mathbf{S}_2$ derives from the linearity of the expectation. The covariance matrices \mathbf{U} and \mathbf{V} are non-identifiable: for any scale factor $s > 0$, we have $\mathcal{MN}(\mathbf{M}, \mathbf{U}, \mathbf{V})$ equals $\mathcal{MN}(\mathbf{M}, s\mathbf{U}, \frac{1}{s}\mathbf{V})$. Therefore, we constrain the parameters such that $\text{Tr}(\mathbf{V}) = 1$. The covariance matrices verify (see e.g. Section 1 in the supplement of [10])

$$\begin{aligned} \mathbf{U} &= \mathbb{E}[(\mathbf{W} - \mathbf{M})(\mathbf{W} - \mathbf{M})^\top] \\ \mathbf{V} &= \frac{1}{\text{Tr}(\mathbf{U})} \mathbb{E}[(\mathbf{W} - \mathbf{M})^\top (\mathbf{W} - \mathbf{M})]. \end{aligned}$$

The Walsh-Hadamard matrix \mathbf{H} is symmetric. Denoting by $\boldsymbol{\Sigma}^{1/2}$ a root of $\boldsymbol{\Sigma}$ and considering $\boldsymbol{\epsilon} \sim \mathcal{N}(\mathbf{0}, \mathbf{I})$, we have

$$\mathbf{U} = \mathbb{E} \left[\mathbf{S}_1 \mathbf{H} \text{diag}(\boldsymbol{\Sigma}^{1/2} \boldsymbol{\epsilon}) \mathbf{H} \mathbf{S}_2^2 \mathbf{H} \text{diag}(\boldsymbol{\Sigma}^{1/2} \boldsymbol{\epsilon}) \mathbf{H} \mathbf{S}_1 \right]. \quad (9)$$

If we define the matrix $\mathbf{T}_2 \in \mathbb{R}^{D \times D^2}$ where the i^{th} row is the column-wise vectorization of the matrix $(\boldsymbol{\Sigma}_{i,j}^{1/2} (\mathbf{H} \mathbf{S}_2)_{i,j'})_{j,j' \leq D}$. We have

$$\begin{aligned} (\mathbf{T}_2 \mathbf{T}_2^\top)_{i,i'} &= \sum_{j,j'=1}^D \boldsymbol{\Sigma}_{i,j}^{1/2} \boldsymbol{\Sigma}_{i',j'}^{1/2} (\mathbf{H} \mathbf{S}_2)_{i,j'} (\mathbf{H} \mathbf{S}_2)_{i',j'} \\ &= \sum_{j,j',j''=1}^D \boldsymbol{\Sigma}_{i,j}^{1/2} (\mathbf{H} \mathbf{S}_2)_{i,j'} \mathbb{E}[\epsilon_j \epsilon_{j''}] \boldsymbol{\Sigma}_{i',j''}^{1/2} (\mathbf{H} \mathbf{S}_2)_{i',j''} \\ &= \sum_{j'=1}^D \mathbb{E} \left[\left(\sum_{j=1}^D \epsilon_j \boldsymbol{\Sigma}_{i,j}^{1/2} (\mathbf{H} \mathbf{S}_2)_{i,j'} \right) \left(\sum_{j''=1}^D \epsilon_{j''} \boldsymbol{\Sigma}_{i',j''}^{1/2} (\mathbf{H} \mathbf{S}_2)_{i',j'} \right) \right] \\ &= \mathbb{E} \left[\left(\text{diag}(\boldsymbol{\Sigma}^{1/2} \boldsymbol{\epsilon}) \mathbf{H} \mathbf{S}_2^2 \mathbf{H} \text{diag}(\boldsymbol{\Sigma}^{1/2} \boldsymbol{\epsilon}) \right)_{i,i'} \right]. \end{aligned}$$

Using (9), a root of $\mathbf{U} = \mathbf{U}^{1/2} \mathbf{U}^{1/2\top}$ can be found:

$$\mathbf{U}^{1/2} = \mathbf{S}_1 \mathbf{H} \mathbf{T}_2. \quad (10)$$

Similarly for \mathbf{V} , we have

$$\begin{aligned} \mathbf{V}^{1/2} &= \frac{1}{\sqrt{\text{Tr}(\mathbf{U})}} \mathbf{S}_2 \mathbf{H} \mathbf{T}_1, \\ \text{with } \mathbf{T}_1 &= \begin{bmatrix} \text{vect} \left(\boldsymbol{\Sigma}_{1,:} (\mathbf{H} \mathbf{S}_1)_{1,:}^\top \right)^\top \\ \vdots \\ \text{vect} \left(\boldsymbol{\Sigma}_{D,:} (\mathbf{H} \mathbf{S}_1)_{D,:}^\top \right)^\top \end{bmatrix}. \end{aligned} \quad (11)$$

B Geometric Interpretation of WHVI

The matrix \mathbf{A} in Section 2.2 expresses the linear relationship between the weights $\mathbf{W} = \mathbf{S}_1 \mathbf{H} \mathbf{G} \mathbf{H} \mathbf{S}_2$ and the variational random vector \mathbf{g} , i.e. $\text{vect}(\mathbf{W}) = \mathbf{A} \mathbf{g}$. Recall the definition of

$$\mathbf{A} = \begin{bmatrix} \mathbf{S}_1 \mathbf{H} \text{diag}(\mathbf{v}_1) \\ \vdots \\ \mathbf{S}_1 \mathbf{H} \text{diag}(\mathbf{v}_D) \end{bmatrix}, \quad \text{with } \mathbf{v}_i = (\mathbf{S}_2)_{i,i} (\mathbf{H})_{:,i}. \quad (12)$$

We show that a \mathbf{LQ} -decomposition of \mathbf{A} can be explicitly formulated.

Proposition. Let A be a $D^2 \times D$ matrix such that $\text{vect}(\mathbf{W}) = \mathbf{A}\mathbf{g}$, where \mathbf{W} is given by $\mathbf{W} = \mathbf{S}_1 \mathbf{H} \text{diag}(\mathbf{g}) \mathbf{H} \mathbf{S}_2$. Then a \mathbf{LQ} -decomposition of A can be formulated as

$$\begin{aligned} \text{vect}(\mathbf{W}) &= [s_i^{(2)} \mathbf{S}_1 \mathbf{H} \text{diag}(\mathbf{h}_i)]_{i=1, \dots, D} \mathbf{g} \\ &= \mathbf{L} \mathbf{Q} \mathbf{g}, \end{aligned} \quad (13)$$

where \mathbf{h}_i is the i^{th} column of \mathbf{H} , $\mathbf{L} = \text{diag}((s_i^{(2)} \mathbf{s})_{i=1, \dots, D})$, $\text{diag}(\mathbf{s}^{(1)}) = \mathbf{S}_1$, $\text{diag}(\mathbf{s}^{(2)}) = \mathbf{S}_2$, and $\mathbf{Q} = [\mathbf{H} \text{diag}(\mathbf{h}_i)]_{i=1, \dots, D}$.

Proof. Equation (13) derives directly from block matrix and vector operations. As \mathbf{L} is clearly lower triangular (even diagonal), let us proof that \mathbf{Q} has orthogonal columns. Defining the $d \times d$ matrix $\mathbf{Q}^{(i)} = \mathbf{H} \text{diag}(\mathbf{h}_i)$, we have:

$$\begin{aligned} \mathbf{Q}^\top \mathbf{Q} &= \sum_{i=1}^D \mathbf{Q}^{(i)\top} \mathbf{Q}^{(i)} \\ &= \sum_{i=1}^D \text{diag}(\mathbf{h}_i) \mathbf{H}^\top \mathbf{H} \text{diag}(\mathbf{h}_i) \\ &= \sum_{i=1}^D \text{diag}(\mathbf{h}_i^2) = \sum_{i=1}^D \frac{1}{D} \mathbf{I} = \mathbf{I}. \end{aligned}$$

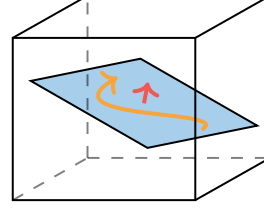


Figure 10: Diagrammatic representation of WHVI. The cube represent the high dimensional parameter space. The variational posterior (mean in orange) evolves during optimization in the (blue) subspace whose orientation (red) is controlled by \mathbf{S}_1 and \mathbf{S}_2 .

This decomposition gives direct insight on the role of the Walsh-Hadamard transforms: with complexity $D \log(D)$, they perform fast rotations \mathbf{Q} of vectors living in a space of dimension D (the plane in Fig. 10) into a space of dimension D^2 (the cube in Figure 10). Treated as parameters gathered in \mathbf{L} , \mathbf{S}_1 and \mathbf{S}_2 control the orientation of the subspace by distortion of the canonical axes.

We empirically evaluate the minimum RMSE, as a proxy for some measure of average distance, between \mathbf{W} and any given point $\mathbf{\Gamma}$. More precisely, we compute for $\mathbf{\Gamma} \in \mathbb{R}^{D \times D}$,

$$\min_{\mathbf{s}_1, \mathbf{s}_2, \mathbf{g} \in \mathbb{R}^D} \frac{1}{D} \|\mathbf{\Gamma} - \text{diag}(\mathbf{s}_1) \mathbf{H} \text{diag}(\mathbf{g}) \mathbf{H} \text{diag}(\mathbf{s}_2)\|_{\text{Frob}}. \quad (14)$$

Fig. 11 shows this quantity evaluated for $\mathbf{\Gamma}$ sampled with i.i.d. $\mathcal{U}(-1, 1)$ with increasing value of D . The bounded behavior suggests that WHVI can approximate any given matrices with a precision that does not increase with the dimension.

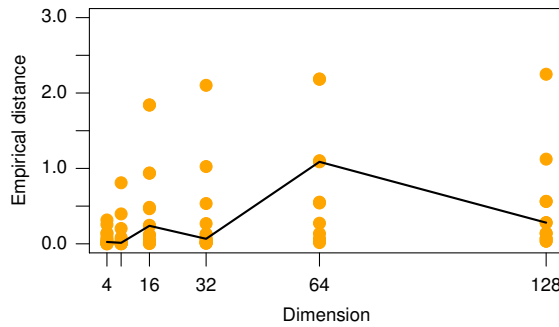


Figure 11: Distribution of the minimum RMSE between $\mathbf{S}_1 \mathbf{H} \mathbf{G} \mathbf{H} \mathbf{S}_2$ and a sample matrix with i.i.d. $\mathcal{U}(-1, 1)$ entries. For each dimension, the orange dots represent 20 repetitions. The median distance is displayed in black. Few outliers (with distance greater than 3.0) appeared, possibly due to imperfect numerical optimization. They were kept for the calculation of the median but not displayed.

C Additional Details on Normalizing Flows

In the general setting, given a probabilistic model with observations \mathbf{x} , latent variables \mathbf{z} and model parameters θ , by introducing an approximate posterior distribution $q_\phi(\mathbf{z})$ with parameters ϕ , the variational lower bound to the log-marginal likelihood is defined as

$$\begin{aligned} \text{KL}\{q_\phi(\mathbf{z})||p(\mathbf{z}|\mathbf{x})\} &= \mathbb{E}_{q_\phi(\mathbf{z})} [\log q_\phi(\mathbf{z}) - \log p(\mathbf{z}|\mathbf{x})] \\ &= \mathbb{E}_{q_\phi(\mathbf{z})} [\log q_\phi(\mathbf{z}) - \log p_\theta(\mathbf{x}, \mathbf{z}) - \log p(\mathbf{x})] \\ &\leq -\mathbb{E}_{q_\phi(\mathbf{z})} [\log p_\theta(\mathbf{x}|\mathbf{z}) - \log q_\phi(\mathbf{z}) + \log p(\mathbf{z})] \end{aligned} \quad (15)$$

where $p_\theta(\mathbf{x}|\mathbf{z})$ is the likelihood function with θ model parameters and $p(\mathbf{z})$ is the prior on the latents. The objective is then to minimize the negative variational bound (NELBO):

$$\mathcal{L}(\theta, \phi) = -\mathbb{E}_{q_\phi(\mathbf{z})} \log p_\theta(\mathbf{x}|\mathbf{z}) + \text{KL}\{q_\phi(\mathbf{z})||p(\mathbf{z})\}. \quad (16)$$

Consider an invertible, continuous and differentiable function $f: \mathbb{R}^D \rightarrow \mathbb{R}^D$. Given $\tilde{\mathbf{z}}_0 \sim q(\mathbf{z}_0)$, then $\tilde{\mathbf{z}}_1 = f(\tilde{\mathbf{z}}_0)$ follows $q(\mathbf{z}_1)$ defined as

$$q(\mathbf{z}_1) = q(\mathbf{z}_0) \left| \det \frac{\partial f}{\partial \mathbf{z}_0} \right|^{-1}. \quad (17)$$

As a consequence, after K transformations the log-density of the final distribution is

$$\log q(\mathbf{z}_K) = \log q(\mathbf{z}_0) - \sum_{k=1}^K \log \left| \det \frac{\partial f_{k-1}}{\partial \mathbf{z}_{k-1}} \right|. \quad (18)$$

We shall define $f_k(\mathbf{z}_{k-1}; \lambda_k)$ the k^{th} transformation which takes input from the previous flow \mathbf{z}_{k-1} and has parameters λ_k . The final variational objective is

$$\begin{aligned} \mathcal{L}(\theta, \phi) &= -\mathbb{E}_{q_\phi(\mathbf{z})} [\log p_\theta(\mathbf{x}|\mathbf{z})] + \text{KL}\{q_\phi(\mathbf{z})||p(\mathbf{z})\} \\ &= \mathbb{E}_{q_\phi(\mathbf{z}|\mathbf{x})} [-\log p_\theta(\mathbf{x}|\mathbf{z}) - \log p(\mathbf{z}) + \log q_\phi(\mathbf{z})] \\ &= \mathbb{E}_{q_0(\mathbf{z}_0)} [-\log p_\theta(\mathbf{x}|\mathbf{z}_K) - \log p(\mathbf{z}_K) + \log q_K(\mathbf{z}_K)] \\ &= \mathbb{E}_{q_0(\mathbf{z}_0)} [-\log p_\theta(\mathbf{x}|\mathbf{z}_K) - \log p(\mathbf{z}_K) + \log q_0(\mathbf{z}_0) \\ &\quad - \sum_{k=1}^K \log \left| \det \frac{\partial f_k(\mathbf{z}_{k-1}; \lambda_k)}{\partial \mathbf{z}_{k-1}} \right|] \\ &= -\mathbb{E}_{q_0(\mathbf{z}_0)} \log p_\theta(\mathbf{x}|\mathbf{z}) + \text{KL}\{q_0(\mathbf{z}_0)||p(\mathbf{z}_K)\} \\ &\quad - \mathbb{E}_{q_0(\mathbf{z}_0)} \sum_{k=1}^K \log \left| \det \frac{\partial f_k(\mathbf{z}_{k-1}; \lambda_k)}{\partial \mathbf{z}_{k-1}} \right|. \end{aligned} \quad (19)$$

Setting the initial distribution q_0 to a fully factorized Gaussian $\mathcal{N}(\mathbf{z}_0|\mu, \sigma\mathbf{I})$ and assuming a Gaussian prior on the generated \mathbf{z}_K , the KL term is analytically tractable. A possible family of transformation is the *planar flow* [49]. For the *planar flow*, f is defined as

$$f(\mathbf{z}) = \mathbf{z} + \mathbf{u}h(\mathbf{w}^\top \mathbf{z} + b), \quad (20)$$

where $\lambda = [\mathbf{u} \in \mathbb{R}^D, \mathbf{w} \in \mathbb{R}^D, b \in \mathbb{R}]$ and $h(\cdot) = \tanh(\cdot)$. This is equivalent to a residual layer with single neuron MLP – as argued by Kingma et al. [30]. The log-determinant of the Jacobian of f is

$$\begin{aligned} \log \left| \det \frac{\partial f}{\partial \mathbf{z}} \right| &= \left| \det(\mathbf{I} + \mathbf{u}[h'(\mathbf{w}^\top \mathbf{z} + b)\mathbf{w}]^\top) \right| \\ &= \left| 1 + \mathbf{u}^\top \mathbf{w} h'(\mathbf{w}^\top \mathbf{z} + b) \right|. \end{aligned} \quad (21)$$

Although this is a simple flow parameterization, a planar flow requires only $\mathcal{O}(D)$ parameters and thus it does not increase the time/space complexity of WHVI. Alternatives can be found in [49, 59, 30, 35].

D Additional Results

D.1 Experimental Setup for Bayesian DNN

The experiments on Bayesian DNN are run with the following setup. For WHVI, we used a zero-mean prior over \mathbf{g} with fully factorized covariance $\lambda \mathbf{I}$; $\lambda = 10^{-5}$ was chosen to obtain sensible variances in the output layer. It is possible to design a prior over \mathbf{g} such that the prior on \mathbf{W} has constant marginal variance and low correlations although empirical evaluations showed not to yield a significant improvement compared to the previous (simpler) choice. In the final implementation of WHVI that we used in all experiments, \mathbf{S}_1 and \mathbf{S}_2 are optimized. The dropout rate of MCD is set to 0.005. We used classic Gaussian likelihood with optimized noise variance for regression and softmax likelihood for classification.

Table 5: List of dataset used in the experiments

NAME	TASK	N.	D-IN	D-OUT
EEG	CLASS.	14980	14	2
MAGIC	CLASS.	19020	10	2
MINIBOO	CLASS.	130064	50	2
LETTER	CLASS.	20000	16	26
DRIVE	CLASS.	58509	48	11
MOCAP	CLASS.	78095	37	5
CIFAR10	CLASS.	60000	$3 \times 28 \times 28$	10
BOSTON	REGR.	506	13	1
CONCRETE	REGR.	1030	8	1
ENERGY	REGR.	768	8	2
KIN8NM	REGR.	8192	8	1
NAVAL	REGR.	11934	16	2
POWERPLANT	REGR.	9568	4	1
PROTEIN	REGR.	45730	9	1
YACHT	REGR.	308	6	1
BOREHOL	REGR.	200000	8	1
HARTMAN6	REGR.	30000	6	1
RASTRIGIN5	REGR.	10000	5	1
ROBOT	REGR.	150000	8	1
OTLCIRCUIT	REGR.	20000	6	1

Training is performed for 500 steps with fixed noise variance and for other 50000 steps with optimized noise variance. Batch size is fixed to 64 and for the estimation of the expected loglikelihood we used 1 Monte Carlo sample at train-time and 64 Monte Carlo samples at test-time. We choose the Adam optimizer [27] with exponential learning rate decay $\lambda_{t+1} = \lambda_0(1 + \gamma t)^{-p}$, with $\lambda_0 = 0.001$, $p = 0.3$, $\gamma = 0.0005$ and t being the current iteration.

Similar setup was also used for the Bayesian CNN experiment. The only differences are the batch size – increased to 256 – and the optimizer, which is run without learning rate decay.

D.2 Regression Experiments on Shallow Models

For a complete experimental evaluation of WHVI, we also use the experimental setup proposed by Hernandez-Lobato and Adams [23] and adopted in several other works [15, 34, 66]. In this configuration, we use one hidden layer with 50 hidden units for all datasets with the exception of PROTEIN where the number of units is increased to 100. Results are reported in Table 6.

Table 6: Test RMSE and test MNLL for regression datasets following the setup in [23].

MODEL DATASET	TEST ERROR				TEST MNLL			
	MCD	MFG	NNG	WHVI	MCD	MFG	NNG	WHVI
BOSTON	3.40 (0.66)	3.04 (0.64)	2.74 (0.12)	2.56 (0.15)	5.04 (1.76)	3.19 (0.89)	2.45 (0.03)	2.55 (0.15)
CONCRETE	4.60 (0.53)	5.24 (0.53)	5.02 (0.12)	5.01 (0.25)	2.96 (0.23)	3.03 (0.15)	3.04 (0.02)	2.95 (0.06)
ENERGY	1.18 (0.03)	1.52 (0.09)	0.48 (0.02)	1.20 (0.07)	3.00 (0.07)	3.49 (0.11)	1.42 (0.00)	3.01 (0.12)
KIN8NM	0.09 (0.00)	0.10 (0.00)	0.08 (0.00)	0.12 (0.01)	-1.09 (0.04)	-1.01 (0.04)	-1.15 (0.00)	-0.78 (0.10)
NAVAL	0.00 (0.00)	0.01 (0.00)	0.00 (0.00)	0.01 (0.00)	-9.93 (0.01)	-6.48 (0.02)	-7.08 (0.03)	-6.25 (0.01)
POWERPLANT	4.20 (0.12)	4.23 (0.13)	3.89 (0.04)	4.11 (0.12)	2.76 (0.03)	2.77 (0.03)	2.78 (0.01)	2.74 (0.03)
PROTEIN	4.35 (0.04)	4.74 (0.05)	4.10 (0.00)	4.64 (0.07)	2.80 (0.01)	2.89 (0.01)	2.84 (0.00)	2.86 (0.01)
YACHT	1.72 (0.32)	1.78 (0.45)	0.98 (0.08)	0.96 (0.20)	2.73 (0.74)	2.02 (0.46)	2.32 (0.00)	1.28 (0.22)

Table 10: Complexity table for GPs with random feature and inducing points approximations. In the case of random features, we include both the complexity of computing random features and the complexity of treating the linear combination of the weights variationally (using VI and WHVI).

	SPACE	COMPLEXITY	TIME
MEAN FIELD - RF		$\mathcal{O}(D_{\text{IN}} N_{\text{RF}}) + \mathcal{O}(N_{\text{RF}} D_{\text{OUT}})$	$\mathcal{O}(D_{\text{IN}} N_{\text{RF}}) + \mathcal{O}(N_{\text{RF}} D_{\text{OUT}})$
WHVI - RF		$\mathcal{O}(D_{\text{IN}} N_{\text{RF}}) + \mathcal{O}(\sqrt{N_{\text{RF}}} D_{\text{OUT}})$	$\mathcal{O}(D_{\text{IN}} N_{\text{RF}}) + \mathcal{O}(D_{\text{OUT}} \log N_{\text{RF}})$
INDUCING POINTS		$\mathcal{O}(M)$	$\mathcal{O}(M^3)$

Note: M is the number of pseudo-data/inducing points and N_{RF} is the number of random features used in the kernel approximation.

D.3 ConvNets architectures

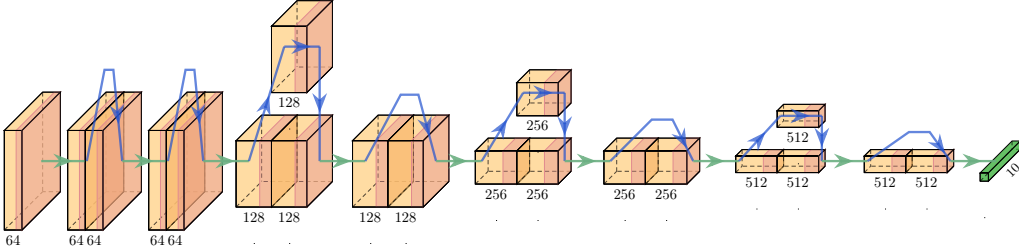


Figure 12: Architecture layout of RESNET 18.

For the experiments on Bayesian convolutional neural networks, we used architectures adapted to CIFAR10 (see Tables 7, 8 and 9).

Table 7: ALEXNET

LAYER	DIMENSIONS
CONV	$64 \times 3 \times 3 \times 3$
MAXPOOL	
CONV	$192 \times 64 \times 3 \times 3$
MAXPOOL	
CONV	$384 \times 192 \times 3 \times 3$
CONV	$256 \times 384 \times 3 \times 3$
CONV	$256 \times 256 \times 3 \times 3$
MAXPOOL	
LINEAR	4096×4096
LINEAR	4096×4096
LINEAR	10×4096

Table 8: VGG16

LAYER	DIMENSIONS
CONV	$32 \times 3 \times 3 \times 3$
CONV	$32 \times 32 \times 3 \times 3$
MAXPOOL	
CONV	$64 \times 32 \times 3 \times 3$
CONV	$64 \times 64 \times 3 \times 3$
MAXPOOL	
CONV	$128 \times 64 \times 3 \times 3$
CONV	$128 \times 128 \times 3 \times 3$
CONV	$128 \times 128 \times 3 \times 3$
MAXPOOL	
CONV	$256 \times 128 \times 3 \times 3$
CONV	$256 \times 256 \times 3 \times 3$
CONV	$256 \times 256 \times 3 \times 3$
MAXPOOL	
CONV	$256 \times 256 \times 3 \times 3$
CONV	$256 \times 256 \times 3 \times 3$
CONV	$256 \times 256 \times 3 \times 3$
MAXPOOL	
LINEAR	10×256

Table 9: RESNET 18

LAYER	DIMENSIONS
RESNET BLOCK	$\begin{bmatrix} 3 \times 3, 64 \\ 3 \times 3, 64 \end{bmatrix} \times 2$
RESNET BLOCK	$\begin{bmatrix} 3 \times 3, 128 \\ 3 \times 3, 128 \end{bmatrix} \times 2$
RESNET BLOCK	$\begin{bmatrix} 3 \times 3, 256 \\ 3 \times 3, 256 \end{bmatrix} \times 2$
RESNET BLOCK	$\begin{bmatrix} 3 \times 3, 512 \\ 3 \times 3, 512 \end{bmatrix} \times 2$
AVGPOOL	
LINEAR	10×512

D.4 Results - Gaussian Processes with Random Feature Expansion

We test WHVI for scalable GP inference, by focusing on GPs with random feature expansions [32]. In GP models, latent variables \mathbf{f} are given a prior $p(\mathbf{f}) = \mathcal{N}(\mathbf{0}|\mathbf{K})$; the assumption of zero mean can be easily relaxed. Given a random feature expansion of the kernel matrix, say $\mathbf{K} \approx \Phi\Phi^\top$, the latent variables can be rewritten as:

$$\mathbf{f} = \Phi\mathbf{w} \quad (22)$$

with $\mathbf{w} \sim \mathcal{N}(\mathbf{0}, \mathbf{I})$. The random features Φ are constructed by randomly projecting the input matrix \mathbf{X} using a Gaussian random matrix Ω and applying a nonlinear transformation, which depends on the

choice of the kernel function. The resulting model is now linear, and considering regression problems such that $\mathbf{y} = \mathbf{f} + \varepsilon$ with $\varepsilon \sim \mathcal{N}(\mathbf{0}, \sigma^2 \mathbf{I})$, solving GPs for regression becomes equivalent to solving standard linear regression problems. For a given set of random features, we treat the weights of the resulting linear layer variationally and evaluate the performance of WHVI.

By reshaping the vector of parameters \mathbf{w} of the linear model into a $D \times D$ matrix, WHVI allows for the linearized GP model to reduce the number of parameters to optimize (see Table 10). We compare WHVI with two alternatives; one is VI of the Fourier features GP expansion that uses less random features to match the number of parameters used in WHVI, and another is the sparse Gaussian process implementation of GPFLOW [38] with a number of inducing points (rounded up) to match the number of parameters used in WHVI.

We report the results on five datasets ($10000 \leq N \leq 200000$, $5 \leq D \leq 8$, see Table 5). The data sets are generated from space-filling evaluations of well known functions in analysis of computer experiments (see e.g. [56]). Dataset splitting in training and testing points is random uniform, 20% versus 80 %. The input variables are rescaled between 0 and 1. The output values are standardized for training. All GPs have the same prior (centered GP with RBF covariance), initialized with equal hyperparameter values: each of the D lengthscales to $\sqrt{D/2}$, the GP variance to 1, the Gaussian likelihood standard deviation to 0.02 (prior observation noise). The training is performed with 12000 steps of Adam optimizer. The observation noise is fixed for the first 10000 steps. Learning rate is 6×10^{-4} , except for the dataset HARTMAN6 with a learning rate of 5×10^{-3} . Sparse GPs are run with whitened representation of the inducing points.

The results are shown in Fig. 13 with diagonal covariance for the three variational posteriors and with full covariance. In both mean field and full covariance settings, this variant of WHVI using the reshaping of \mathbf{W} into a column largely outperforms the direct VI of Fourier features. However, it appears that this improvement of the random feature inference for GPs is not enough to reach the performance of VI using inducing points. Inducing point approximations are based on the Nystroöm approximation of kernel matrices, which are known to lead to lower approximation error on the elements on the kernel matrix compared to random features approximations. This is the reason we attribute to the lower performance of WHVI compared to inducing points approximations in this experiment.

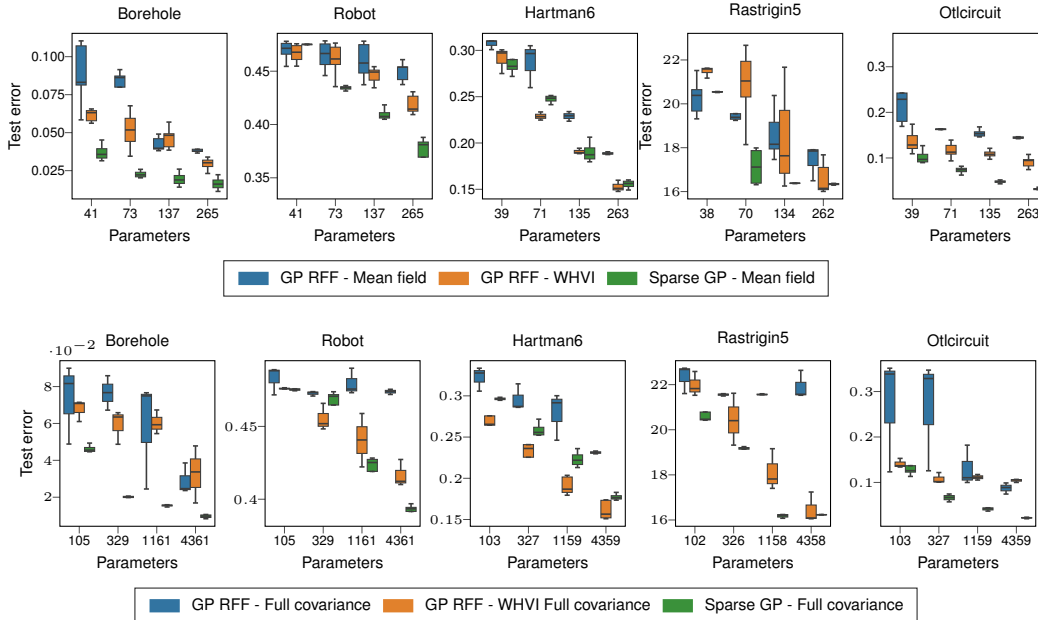


Figure 13: Comparison of test error w.r.t. the number model parameters (*top*: mean field, *bottom*: full covariance).

D.5 Extended results - DNNs

Being able to increase width and depth of a model without drastically increasing the number of variational parameters is one of the competitive advantages of WHVI. Fig. 14 shows the behavior of WHVI for different network configurations. At test time, increasing the number of hidden layers and the numbers of hidden features allow the model to avoid overfitting while delivering better performance. This evidence is also supported by the analysis of the test MNLL during optimization of the ELBO, as showed in Fig. 15.

Thanks to WHVI structure of the weights matrices, expanding and deepening the model is beneficial not only at convergence but during the entire learning procedure as well. Furthermore, the derived NELBO is still a valid lower bound of the true marginal likelihood and, therefore, a suitable objective function for model selection. Differently from the issue addressed in [50], during our experiments we didn't experience problems regarding initialization of variational parameters. We claim that this is possible thanks to both the reduced number of parameters and the effect of the Walsh-Hadamard transform.

Timing profiling of the Fast Walsh-Hadamard transform Key to the log-linear time complexity is the Fast Walsh-Hadamard transform, which allows to perform the operation $\mathbf{H}\mathbf{x}$ in $\mathcal{O}(D \log D)$ time without requiring to generate and store \mathbf{H} . For our experimental evaluation, we implemented a FWHT operation in PYTORCH (v. 0.4.1) in C++ and CUDA to leverage the full computational capabilities of modern GPUs. Fig. 17 presents a timing profiling of our implementation versus the naive matmul (batch size of 512 samples and profiling repeated 1000 times). The breakeven point for the CPU implementation is in the neighborhood of 512/1024 features, while on GPU we see FWHT is consistently faster.

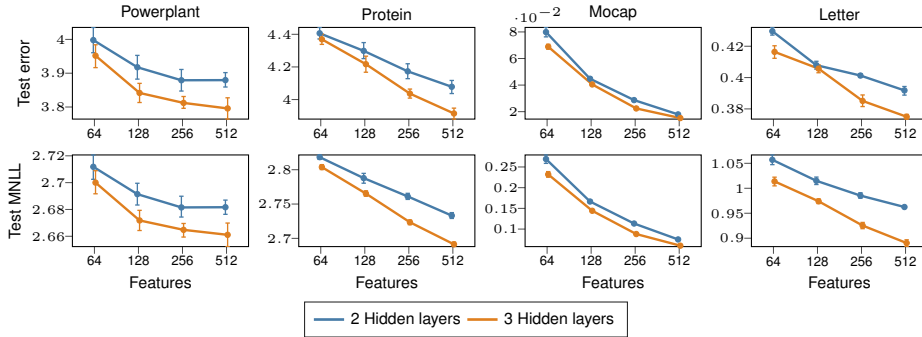


Figure 14: Analysis of model capacity for different features and hidden layers.

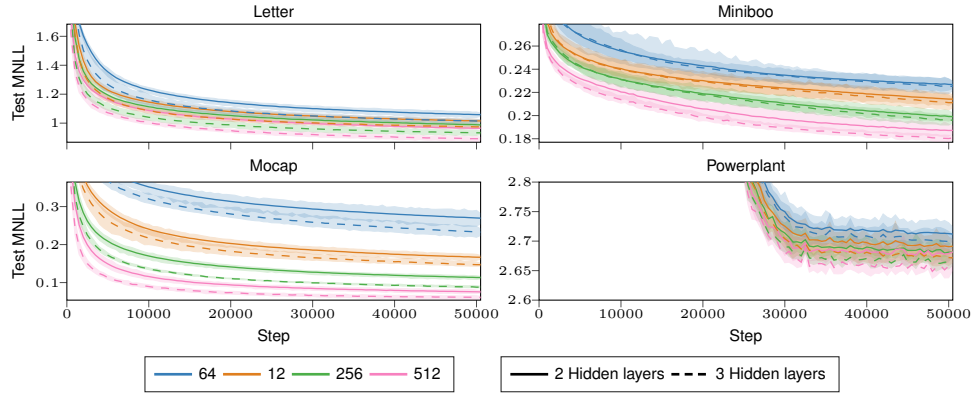


Figure 15: Comparison of test performance. Being able to increase features and hidden layers without worrying about overfitting/overparametrize the model is advantageous not only at convergence but during the entire learning procedure

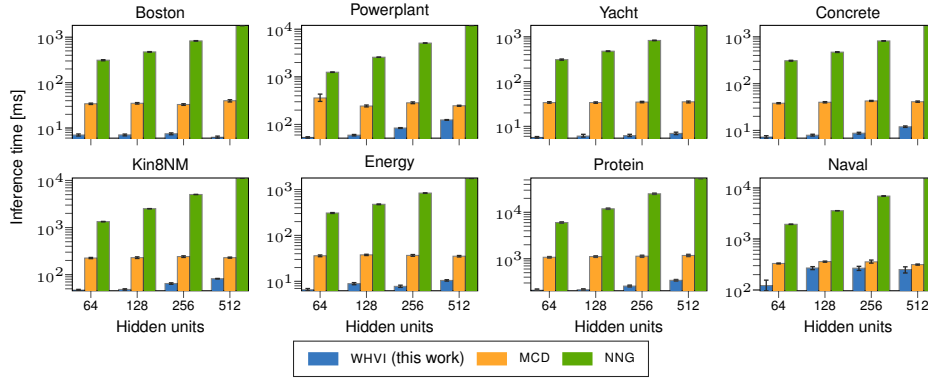


Figure 16: Inference time on the test set with 128 batch size and 64 Monte Carlo samples. Experiment repeated 100 times. Additional datasets available in the Supplement.

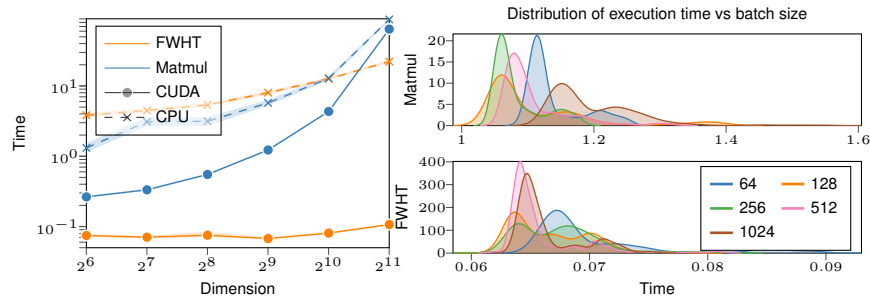


Figure 17: On the (left), time performance versus number of features (D) with batch size fixed to 512. On the (right) distribution of inference time versus batch size ($D=512$) with MATMUL and FWHT on GPU.

Table 11: Test error of Bayesian DNN with 2 hidden layers on regression datasets. NF: number of hidden features

MODEL	DATASET NF	BOSTON	CONCRETE	ENERGY	KIN8NM	NAVAL	POWERPLANT	PROTEIN	TEST ERROR YACHT
MCD	64	3.80 ± 0.88	5.43 ± 0.69	2.13 ± 0.12	0.17 ± 0.22	0.07 ± 0.00	–	4.36 ± 0.12	2.02 ± 0.51
	128	3.91 ± 0.86	5.12 ± 0.79	2.07 ± 0.11	0.09 ± 0.00	0.30 ± 0.30	3.97 ± 0.14	4.23 ± 0.10	1.90 ± 0.54
	256	3.62 ± 1.01	5.03 ± 0.74	2.04 ± 0.11	0.10 ± 0.00	0.07 ± 0.00	3.91 ± 0.11	4.09 ± 0.11	2.09 ± 0.66
	512	3.56 ± 0.85	4.81 ± 0.79	2.03 ± 0.12	0.09 ± 0.00	0.07 ± 0.00	3.90 ± 0.10	3.87 ± 0.11	2.09 ± 0.55
MFG	64	4.06 ± 0.72	6.87 ± 0.54	2.42 ± 0.12	0.11 ± 0.00	0.01 ± 0.00	4.38 ± 0.12	4.85 ± 0.12	4.31 ± 0.62
	128	4.47 ± 0.85	8.01 ± 0.41	3.10 ± 0.14	0.12 ± 0.00	0.01 ± 0.00	4.52 ± 0.13	4.93 ± 0.11	7.01 ± 1.22
	256	5.27 ± 0.98	9.41 ± 0.54	4.03 ± 0.10	0.13 ± 0.00	0.01 ± 0.00	4.79 ± 0.12	5.07 ± 0.12	8.71 ± 1.31
	512	6.04 ± 0.90	10.84 ± 0.46	4.90 ± 0.11	0.16 ± 0.00	0.01 ± 0.00	5.53 ± 0.16	5.26 ± 0.10	10.34 ± 1.45
NNG	64	3.20 ± 0.26	6.90 ± 0.59	1.54 ± 0.18	0.07 ± 0.00	0.00 ± 0.00	3.94 ± 0.05	3.90 ± 0.02	3.57 ± 0.70
	128	3.56 ± 0.43	8.21 ± 0.55	1.96 ± 0.28	0.07 ± 0.00	0.00 ± 0.00	4.23 ± 0.09	4.57 ± 0.47	5.16 ± 1.48
	256	4.87 ± 0.94	8.18 ± 0.57	3.41 ± 0.55	0.07 ± 0.00	0.00 ± 0.00	4.07 ± 0.00	4.88 ± 0.00	5.60 ± 0.65
	512	5.19 ± 0.62	11.67 ± 2.06	5.12 ± 0.37	0.10 ± 0.00	0.00 ± 0.00	4.97 ± 0.00	–	5.91 ± 0.80
WHVI	64	3.33 ± 0.82	5.24 ± 0.77	0.73 ± 0.11	0.08 ± 0.00	0.01 ± 0.00	4.07 ± 0.11	4.49 ± 0.12	0.82 ± 0.18
	128	3.14 ± 0.71	4.70 ± 0.72	0.58 ± 0.07	0.08 ± 0.00	0.01 ± 0.00	4.00 ± 0.12	4.36 ± 0.11	0.69 ± 0.16
	256	2.99 ± 0.85	4.63 ± 0.78	0.52 ± 0.07	0.08 ± 0.00	0.01 ± 0.00	3.95 ± 0.12	4.24 ± 0.11	0.76 ± 0.13
	512	2.99 ± 0.69	4.51 ± 0.80	0.51 ± 0.04	0.07 ± 0.00	0.01 ± 0.00	3.96 ± 0.12	4.14 ± 0.09	0.71 ± 0.16

Table 12: Test MNLL of Bayesian DNN with 2 hidden layers on regression datasets. NF: number of hidden features

MODEL	DATASET NF	BOSTON	CONCRETE	ENERGY	KIN8NM	NAVAL	POWERPLANT	PROTEIN	TEST MNLL YACHT
MCD	64	5.67 ± 2.35	3.19 ± 0.28	4.19 ± 0.15	–0.78 ± 0.69	–2.68 ± 0.00	–	2.79 ± 0.01	2.85 ± 1.02
	128	6.90 ± 2.93	3.20 ± 0.36	4.15 ± 0.15	–0.87 ± 0.02	–1.00 ± 2.27	2.74 ± 0.05	2.76 ± 0.02	2.95 ± 1.27
	256	6.60 ± 3.59	3.31 ± 0.45	4.13 ± 0.15	–0.70 ± 0.05	–2.70 ± 0.00	2.75 ± 0.04	2.72 ± 0.01	3.79 ± 1.88
	512	7.28 ± 3.31	3.45 ± 0.59	4.13 ± 0.17	–0.76 ± 0.03	–2.71 ± 0.00	2.77 ± 0.04	2.68 ± 0.02	3.76 ± 1.65
MFG	64	2.83 ± 0.33	3.26 ± 0.08	4.42 ± 0.10	–0.92 ± 0.02	–6.24 ± 0.01	2.80 ± 0.03	2.90 ± 0.01	2.85 ± 0.24
	128	2.99 ± 0.41	3.41 ± 0.05	4.91 ± 0.09	–0.83 ± 0.02	–6.23 ± 0.01	2.83 ± 0.03	2.92 ± 0.01	3.38 ± 0.29
	256	3.33 ± 0.53	3.57 ± 0.07	5.44 ± 0.05	–0.69 ± 0.01	–6.22 ± 0.01	2.89 ± 0.02	2.95 ± 0.01	3.65 ± 0.32
	512	3.69 ± 0.54	3.73 ± 0.05	5.83 ± 0.05	–0.49 ± 0.01	–6.19 ± 0.01	3.04 ± 0.03	2.98 ± 0.01	3.86 ± 0.31
NNG	64	2.69 ± 0.06	3.40 ± 0.15	1.95 ± 0.08	–1.14 ± 0.05	–5.83 ± 1.49	2.80 ± 0.01	2.78 ± 0.01	2.71 ± 0.17
	128	2.72 ± 0.09	3.56 ± 0.08	2.11 ± 0.12	–1.19 ± 0.04	–6.52 ± 0.09	2.86 ± 0.02	2.95 ± 0.12	3.06 ± 0.27
	256	3.04 ± 0.22	3.52 ± 0.07	2.64 ± 0.17	–1.19 ± 0.03	–5.73 ± 0.21	2.84 ± 0.00	3.02 ± 0.01	3.15 ± 0.13
	512	3.13 ± 0.14	3.91 ± 0.20	3.07 ± 0.07	–0.80 ± 0.00	–5.30 ± 0.05	3.51 ± 0.00	–	3.21 ± 0.14
WHVI	64	3.68 ± 1.40	3.19 ± 0.34	2.18 ± 0.37	–1.13 ± 0.02	–6.25 ± 0.01	2.73 ± 0.03	2.82 ± 0.01	2.56 ± 1.33
	128	4.33 ± 1.80	3.17 ± 0.37	2.06 ± 0.62	–1.19 ± 0.04	–6.25 ± 0.01	2.71 ± 0.03	2.79 ± 0.01	1.80 ± 1.01
	256	4.99 ± 2.65	3.35 ± 0.59	2.00 ± 0.70	–1.23 ± 0.04	–6.25 ± 0.01	2.70 ± 0.03	2.77 ± 0.01	1.53 ± 0.53
	512	5.41 ± 2.30	3.33 ± 0.56	2.05 ± 0.46	–1.22 ± 0.04	–6.25 ± 0.01	2.70 ± 0.03	2.74 ± 0.01	1.37 ± 0.57

Table 13: Results of Bayesian DNN on 6 classification datasets. Note: NL: number of hidden layers, NF: number of hidden features

MODEL	NL	DATASET	TEST ERROR						TEST MNLL					
			DRIVE	EEG	LETTER	MAGIC	MINIBOO	MOCAP	DRIVE	EEG	LETTER	MAGIC	MINIBOO	MOCAP
MCD	2	64	0.19 ± 0.11	0.16 ± 0.01	0.45 ± 0.05	0.13 ± 0.02	0.07 ± 0.00	0.02 ± 0.02	0.52 ± 0.24	0.36 ± 0.02	1.27 ± 0.26	0.37 ± 0.12	0.18 ± 0.00	0.11 ± 0.10
		128	0.17 ± 0.07	0.19 ± 0.11	0.45 ± 0.04	0.16 ± 0.08	0.15 ± 0.21	0.04 ± 0.07	0.47 ± 0.19	0.36 ± 0.09	1.39 ± 0.22	0.33 ± 0.04	0.24 ± 0.17	0.10 ± 0.11
		256	0.16 ± 0.09	0.20 ± 0.15	0.45 ± 0.06	0.13 ± 0.01	0.07 ± 0.00	0.16 ± 0.13	0.50 ± 0.29	0.33 ± 0.08	1.32 ± 0.25	0.35 ± 0.09	0.17 ± 0.00	0.29 ± 0.21
	3	512	0.18 ± 0.11	0.18 ± 0.15	0.44 ± 0.02	0.18 ± 0.10	0.07 ± 0.00	0.03 ± 0.06	0.47 ± 0.27	0.95 ± 1.63	1.41 ± 0.17	0.40 ± 0.06	0.20 ± 0.04	0.17 ± 0.22
		64	0.34 ± 0.10	0.13 ± 0.01	0.50 ± 0.06	0.16 ± 0.07	0.08 ± 0.02	0.09 ± 0.09	0.88 ± 0.25	0.55 ± 0.61	1.56 ± 0.28	0.42 ± 0.16	0.20 ± 0.05	0.18 ± 0.15
		128	0.32 ± 0.10	0.21 ± 0.14	0.48 ± 0.09	0.16 ± 0.07	0.23 ± 0.28	0.11 ± 0.19	0.86 ± 0.28	1.46 ± 2.78	1.40 ± 0.34	0.44 ± 0.13	0.28 ± 0.18	0.34 ± 0.28
WHVI	2	256	0.32 ± 0.21	0.23 ± 0.17	0.43 ± 0.05	0.14 ± 0.00	0.23 ± 0.28	0.28 ± 0.26	0.87 ± 0.51	0.40 ± 0.09	1.34 ± 0.19	0.62 ± 0.07	0.31 ± 0.22	0.61 ± 0.48
		512	0.36 ± 0.09	0.14 ± 0.11	0.49 ± 0.06	0.14 ± 0.01	0.23 ± 0.28	0.23 ± 0.12	0.93 ± 0.27	0.74 ± 0.78	1.92 ± 0.23	1.02 ± 0.15	0.30 ± 0.20	0.45 ± 0.27
		128	0.03 ± 0.01	0.25 ± 0.01	0.43 ± 0.01	0.13 ± 0.01	0.10 ± 0.00	0.08 ± 0.01	0.14 ± 0.04	0.61 ± 0.28	1.07 ± 0.02	0.32 ± 0.02	0.23 ± 0.01	0.28 ± 0.02
	3	256	0.02 ± 0.00	0.21 ± 0.01	0.41 ± 0.01	0.13 ± 0.01	0.09 ± 0.00	0.05 ± 0.00	0.09 ± 0.02	0.45 ± 0.01	1.02 ± 0.02	0.32 ± 0.02	0.22 ± 0.01	0.17 ± 0.01
		512	0.01 ± 0.00	0.19 ± 0.01	0.40 ± 0.01	0.13 ± 0.01	0.08 ± 0.00	0.03 ± 0.00	0.09 ± 0.03	0.76 ± 0.92	0.99 ± 0.01	0.31 ± 0.02	0.20 ± 0.00	0.12 ± 0.01
		64	0.01 ± 0.00	0.17 ± 0.01	0.40 ± 0.01	0.13 ± 0.01	0.08 ± 0.00	0.02 ± 0.00	0.08 ± 0.03	0.52 ± 0.37	0.97 ± 0.01	0.31 ± 0.01	0.19 ± 0.01	0.08 ± 0.01
	3	64	0.03 ± 0.00	0.33 ± 0.05	0.42 ± 0.01	0.13 ± 0.01	0.10 ± 0.00	0.07 ± 0.01	0.12 ± 0.02	0.61 ± 0.05	1.02 ± 0.02	0.32 ± 0.01	0.23 ± 0.01	0.24 ± 0.02
		128	0.02 ± 0.00	0.38 ± 0.09	0.41 ± 0.01	0.13 ± 0.01	0.09 ± 0.00	0.04 ± 0.00	0.09 ± 0.02	0.64 ± 0.07	0.98 ± 0.01	0.31 ± 0.02	0.22 ± 0.01	0.15 ± 0.01
		256	0.05 ± 0.09	0.45 ± 0.01	0.39 ± 0.01	0.13 ± 0.01	0.08 ± 0.00	0.02 ± 0.00	0.20 ± 0.34	0.69 ± 0.00	0.94 ± 0.02	0.31 ± 0.02	0.20 ± 0.01	0.09 ± 0.01
		512	0.01 ± 0.00	0.45 ± 0.01	0.38 ± 0.01	0.13 ± 0.01	0.08 ± 0.00	0.02 ± 0.00	0.05 ± 0.02	0.69 ± 0.00	0.90 ± 0.01	0.32 ± 0.01	0.19 ± 0.01	0.06 ± 0.01